Monitoring and inverse modelling of hydrogeochemical processes during managed aquifer recharge in Southwestern Bangladesh

Rafiq, Muhammad Risalat; Ahmed, Kazi Matin; Rietveld, Louis C.; van Breukelen, Boris M.

DOI
10.1016/j.apgeochem.2022.105472

Publication date
2022

Document Version
Final published version

Published in
Applied Geochemistry

Applied Geochemistry 146 (2022) 105472

Contents lists available at ScienceDirect

Applied Geochemistry

journal homepage: www.elsevier.com/locate/apgeochem

Monitoring and inverse modelling of hydrogeochemical processes during managed aquifer recharge in Southwestern Bangladesh

Muhammad Risalat Rafiq [a,b,*], Kazi Matin Ahmed [c], Louis C. Rietveld [a], Boris M. van Breukelen [a]

[a] Delft University of Technology, Faculty of Civil Engineering and Geosciences, Department of Water Management, Stevinweg 1, 2628 CN, Delft, the Netherlands
[b] University of Barishal, Faculty of Science and Engineering, Department of Geology and Mining, Barishal, 8254, Bangladesh
[c] University of Dhaka, Faculty of Earth and Environmental Sciences, Department of Geology, Dhaka, 1000, Bangladesh

ARTICLE INFO

Editorial handling by Huaming Guo

Keywords:
Managed aquifer recharge
Aquifer storage transfer and recovery
Groundwater quality
Inverse geochemical modelling
Arsenic mobilization

ABSTRACT

Managed Aquifer Recharge (MAR) has been applied as Aquifer Storage, Transfer, and Recovery (ASTR) to provide fresh drinking water for local communities at 99 locations in southwest Bangladesh since 2009. Aerobic freshwater from ponds is filtered and subsequently infiltrated into anaerobic shallow brackish aquifers. At approximately 45% of these sites, relatively higher levels of Fe and As were observed in recovered water, which requires a better understanding of the hydrogeochemical processes that govern the Fe, Mn, and As levels in these MAR systems. Therefore, two representative sites with As above (74 ± 11 μg/L at site GMF11) and below (19 ± 6 μg/L at site JJS91), the Bangladesh drinking water standard of 50 μg/L were weekly monitored on hydrochemical changes from Dec 2017 to Dec 2018. Hydrogeochemical processes occurring during storage were quantified with inverse and forward geochemical mass balance models developed with PHREEQC. The following processes explained the changes in water quality: 1) mixing of infiltration water with native groundwater (~90%:~10%); 2) consumption of O_2 by a) dissolved Fe^{2+} that subsequently precipitated as $Fe(OH)_3$ at GMF11 and by b) dissolved and sedimentary organic matter (OM) at site JJS91; 3) reduction of SO_4 coupled to the oxidation of OM at both sites; and 4) mixing corrosion and freshening induced cation-exchange (Ca sorption; Na desorption) triggering calcite and siderite dissolution at GMF11. Dissolution of these carbonate minerals occurred to a lesser extent at JJS91, while cation exchange (Na sorption; Ca desorption) suggested that the freshwater was displaced by brackish groundwater because of inadequate infiltration at JJS91. Distinct pH values in recovered water reflected the dominance of Fe^{2+} versus OM oxidation. Siderite dissolution led to 4.3 ± 3.1 and 1.0 ± 0.5 mg/L Fe in recovered water at GMF11 and JJS91, respectively. Elevated As and Mn levels in recovered water were caused for max. 20% by mixing with native groundwater and for min. 80% by mobilization processes, mainly by desorption of As from Fe-oxides and by the dissolution of Mn-bearing siderite. Recommendations are provided to improve recovered water quality.

1. Introduction

Communities living in the coastal areas of the Khulna, the Satkhira, and the Bagerhat districts in southwest Bangladesh are confronted with a lack of accessible, safe drinking water. Anthropogenic surface water contamination (Alam et al., 2006; Bhuiyan et al., 2011), rapid population growth (Abedin et al., 2019; Khan et al., 2014), groundwater salinity (Naus et al., 2019a, 2019b), and arsenic (As) contamination (Ayers et al., 2016; Harvey et al., 2002; Nickson et al., 1998) are considered to be the main constraints for safe drinking water availability. Among various available solutions, managed aquifer recharge (MAR) is regarded as a promising water supply option for this region (Barker et al., 2016; Naus et al., 2021; Sultana et al., 2015). MAR is based on the principle of infiltrating surplus (wet season) fresh water in a shallow aquifer for storage and withdrawal during periods of water deficit (dry season) (Missimer and Maliva, 2010; Zuurbier et al., 2017). Local resources are used, making the approach cost-effective and user-friendly (Dillon et al., 2010, 2019; Page et al., 2018; Pyne, 2017). Diverse MAR systems are practiced internationally depending on local hydrogeological conditions (Dillon et al., 2019). Dillon et al. (2019)

* Corresponding author. Delft University of Technology, Faculty of Civil Engineering and Geosciences, Department of Water Management, Stevinweg 1, 2628 CN, Delft, the Netherlands.
E-mail addresses: m.r.rafiq-1@tudelft.nl (M.R. Rafiq), kmahmed@du.ac.bd (K.M. Ahmed), L.C.Rietveld@tudelft.nl (L.C. Rietveld), B.M.vanBreukelen@tudelft.nl (B.M. van Breukelen).

https://doi.org/10.1016/j.apgeochem.2022.105472
Received 4 March 2022; Received in revised form 15 September 2022; Accepted 24 September 2022
Available online 30 September 2022

reported that these MAR applications are broadly divided into the following categories: streambed channel modifications, bank filtration, water spreading, rainwater harvesting, and recharge wells. Among these, the recharge well technique, which includes both aquifer storage and recovery (ASR) and aquifer storage, transfer, and recovery (ASTR), has largely been used for the improvement of drinking water in coastal regions where aquifers occur beneath sealed clay layers (Dillon et al., 2010). ASTR uses separate wells for injection and recovery, whereas ASR uses the same well for both injection and recovery (Dillon et al., 2010; Pyne, 2005, 2017).

At the MAR sites in Bangladesh, fresh surface water is collected from ponds and harvested rooftop rainwater, and stored in confined aquifers using relatively large diameter infiltration wells (Barker et al., 2016; Hasan et al., 2018). The water is stored in shallow brackish to saline aquifers and extracted for drinking purposes on a daily basis when the quality is found suitable as low salinity and As (Hasan et al., 2018). The recovered water has shown improvement in salinity, turbidity, and reduction in E. Coli (counts) compared to the pond water and native groundwater (Sultana et al., 2015). However, changes in Fe and As concentrations have been observed at several MAR systems, and the levels have occasionally exceeded the drinking water regulations (Sultana et al., 2015). This calls for research to understand better the processes controlling As levels in these MAR systems and the potential solutions to prevent the deterioration of water quality by these metals.

MAR systems take advantage of natural water purification processes, e.g., filtration, sorption, and biodegradation during sediment-water interactions in the aquifers (Antoniou et al., 2012; Pyne, 2005). When water is stored in an anoxic aquifer, dissolved oxygen (DO) from the infiltrated surface water oxidizes Fe(II) in native groundwater and converts it into Fe-hydroxides, which are well-known adsorbents for As and Mn removal (Annaduzzaman et al., 2020; Rahman et al., 2014, 2015; van Halem et al., 2010). Appelo et al. (1999) claimed that the adsorption of these metals can also take place on the sedimentary organic matter and clay minerals in addition to Fe-hydroxides. Antoniou et al. (2012) argued that the water quality might deteriorate due to DO consumption by Fe sulfides, Fe, Mn, and sedimentary organic matter. Moreover, the oxidative dissolution of As-containing Fe sulfides can promote the mobilization of Fe, Mn, and As in the recovered water (Fakhreddine et al., 2020; Neil et al., 2012; Wallis et al., 2011). In addition, these metals can also mobilize due to the reductive dissolution of the Fe hydroxides (Neil et al., 2012; Stuyfzand, 1998; Wallis et al., 2010). These processes can alter the water quality during MAR and restrict safe water production by elevated concentrations of Fe, Mn, and As (Antoniou et al., 2012; Fakhreddine et al., 2021; Neil et al., 2012).

Models are often required to deduce the governing hydrogeochemical processes controlling water quality changes in MAR systems because of the high dynamics in water fluxes and the potential temporal changes in infiltration water quality. To this end, reactive transport models enable the simulation and prediction of water quality changes in the MAR systems (Antoniou et al., 2013; Fakhreddine et al., 2020; Greskowiak et al., 2005; Wallis et al., 2011). Alternatively, simpler chemical (inverse) mass balance models can be applied to provide fundamental insights into key hydrogeochemical processes affecting groundwater quality changes (Ibrahim and El-Naqa, 2018; Morán-Ramírez et al., 2016; Poetra et al., 2020; van Breukelen et al., 2003). This simpler model has rarely been applied at MAR sites, with the exception of research by Antoniou et al. (2012), who used a spreadsheet mass balance model to determine hydrogeochemical processes at an ASR site in the Netherlands.

Despite the intensive application of MAR in many countries worldwide (Antoniou et al., 2013; Fakhreddine et al., 2021; Wallis et al., 2010; Zuurbier et al., 2016), the number of studies conducted on these ASTR systems in Bangladesh is limited (Naus et al., 2021; Sultana et al., 2015). The mobilization of Fe and As in MAR systems was site-specific and has mostly been studied in moderate climatic areas (Neil et al., 2012). Therefore, the various hydrogeochemical processes that control abstracted water quality were investigated at two representative MAR sites in the coastal area of southwest Bangladesh. The two sites exhibited distinct As levels: GMF11 had As levels above the Bangladesh drinking water standard of 50 mg/L, whereas site JJS91 had As levels below this drinking water standard. These sites were preferred among other MAR sites with comparable As levels after considering the road accessibility, the availability of electricity or power, and the logistical assistance needed for field experiments. To this end, weekly monitoring was conducted on various hydrochemical parameters of pond water, infiltration water (after sand filtration), native groundwater, and abstracted (drinking) water at both sites for one full year. Sediment samples of the aquifers were obtained and analyzed on geochemical properties. Inverse and forward geochemical mass balance models were developed in PHREEQC to simulate the hydrochemical composition of the abstracted water and to determine the key hydrogeochemical processes to explain water quality changes at both sites. Based on the obtained insights, recommendations were formulated for the operation and design of the MAR sites to improve the drinking water quality at these sites.

2. Methods

2.1. Site descriptions

Fig. 1 shows the locations of the two MAR sites named GMF11 (N 22°37′18.05″, E 89°50′09.67″) and JJS91 (N 22°26′30.01″, E 89°48′14.54″) in the coastal area of SW Bangladesh. Both MAR sites use a freshwater pond with a surface area of 7000 m^2 for GMF11 and 3345 m^2 for JJS91 as a source of infiltration water. Both ponds occupy an average depth of approximately 5 m. The ponds used at these two locations (as for most of the other MAR sites in the region) are dug out to an approximate depth of 3–5 m in a confining clay layer having a thickness ranging between 6 and 15 m. As at every site, several meters of clay layer separate the pond water from the aquifer; the hydrological connection between the pond and aquifer is therefore limited. Besides, we did not find any indication of decreasing salinity in shallow aquifers due to the lateral recharge of pondwater, also confirming the limited connection between surface and groundwater. Pond water is pumped to a double-chambered sand filtration tank at about 2 m elevations, filtrated, and subsequently infiltrated by gravity in an anoxic and brackish sandy aquifer, beneath a clay layer of about 12 m thickness for GMF11 and 6 m for JJS91. Six (GMF11) and four (JJS91) large-diameter infiltration wells were used, which were positioned in a circle of 1.8 m radius (Fig. 2 and Fig. S3 in Supplement). The diameter of the infiltration wells varies in casing and screen dimensions for both sites. At site GMF11, the diameter of the PVC casing is 0.25 m and 0.30 m of the screen, whereas, at site JJS91, the diameter of the PVC casing is 0.30 m and 0.45 m of the screen (Fig. 2 and Fig. S3 in Supplement). The depth of each infiltration well is 24.4 m for GMF11 and 22.3 m for JJS91, having 12.2 and 15.2 m long screens, respectively (Fig. 2 and Fig. S3 in Supplement). At both sites, an abstraction well (diameter: 0.05 m; screen length: 3.05 m) was positioned in the system's center. This well is used to abstract the stored freshwater using a hand-operated tube well, occurring at a depth below the surface of 12.2–21.4 m for GMF11 and 6.1–16.8 m for JJS91 (Fig. 2 and Fig. S3 in Supplement). Both sites keep five monitoring wells with diameters and screen lengths similar to the abstraction well. One deep well (center deep well) was installed at a depth of about 26 m for GMF11 and 21 m for JJS91. The other four observation wells (outer shallow wells 3–6) were placed outside the circle of infiltration wells in a 3.66 m radius circle with screens at the same depth as the abstraction well (Fig. 2 and Fig. S3 in Supplement).

2.2. Water sample collection and analyses

Both MAR sites were monitored weekly for a full year starting on December 5, 2017. Samples were collected from the infiltration water (filtered pond water), the aquifer from the outer shallow observation

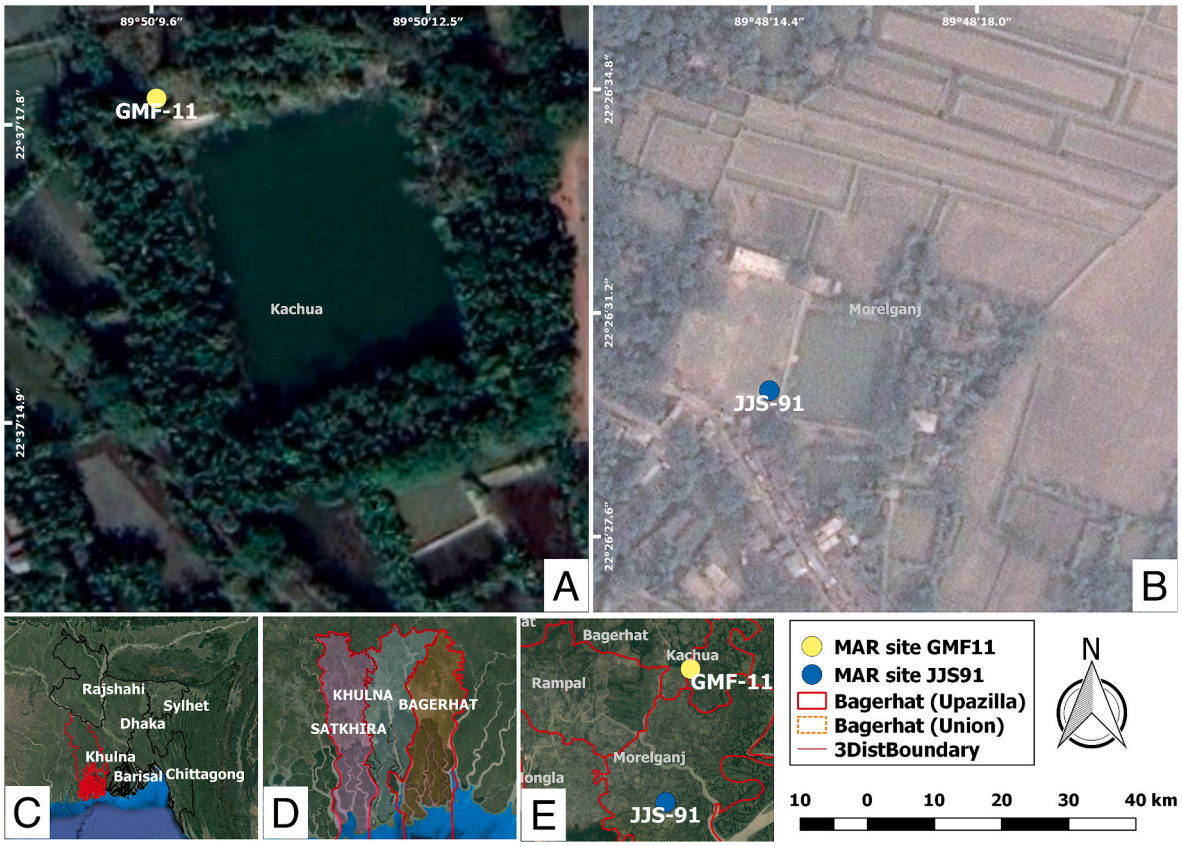

Fig. 1. QGIS (version 2.18.4) prepared map showing the locations of the two MAR sites in the Kachua (GMF11, A) and Morrelganj (JJS91, B) upazilla of Bagerhat, SW Bangladesh (C–E). Two recent satellite photos were used to show the surroundings of the two sites (A–B), including the surface water reservoir (freshwater pond) used as source water. These ponds can be identified from their dark hue and rectangular form, and are indicated by a yellow (GMF11, A) and a blue (JJS91, B) dot from where the water was collected to recharge MAR systems. Site GMF11(A) is surrounded by agricultural lands, while site JJS91(B) is located on the premises of a primary school. (For interpretation of the references to color in this figure legend, the reader is referred to the Web version of this article.)

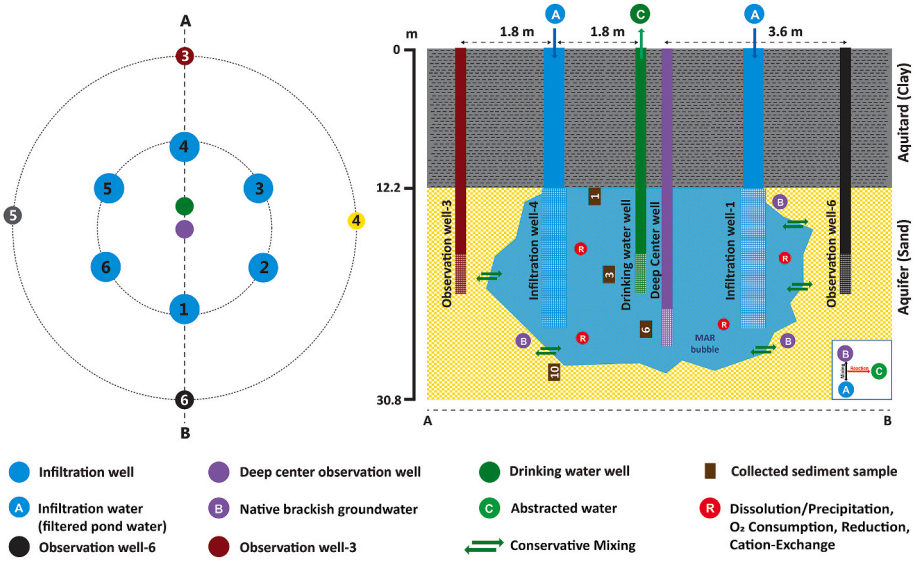

Fig. 2. Schematic layout of site GMF11 in map view (left), and in cross-sectional view depicting the hydrogeological situation (right). The positions and screen lengths of the various wells as well as the depth of collected sediment samples are shown. In addition, schematic of the inverse geochemical model showing abstracted water (C) quality is considered a result of mixing of filtered pond water (A) with native brackish groundwater (B), and additional reactions/processes (R) such as dissolution/precipitation, O_2 consumption, SO_4 reduction, and cation exchange.

well number 6, the center deep well, and the abstraction well (Fig. 2 and Fig. S3 in Supplement). In addition, the other outer observation wells (Fig. 2 and Fig. S3 in Supplement) and the pond water were sampled monthly. Water samples were collected using a submersible pump (Eijkelkamp Gigant®). Before sampling, each well was purged with triple the standing volume of the respective well. Electrical conductivity (EC), temperature, pH/redox, and DO were measured in situ using a PONSEL ODEON® multi-parameter meter (Fig. S4 in Supplement). Individual PONSEL ODEON® sensors were applied for measuring these onsite parameters. For instance, PC4EA was used to measure EC/temperature with graphite and platinum-type electrodes, PPHRA was applied to measure pH/redox/temperature using an Ag/AgCl reference

electrode in a PLASTOGEL® KCl-saturated plasticized electrolyte, and the OPTOD sensor was used to measure DO applying the principle of luminescence-based optical measurement. Besides these parameters, Alkalinity and turbidity were measured using a digital titrator (HACH Method 10244) and a portable turbidity meter (HANNA HI 93703), respectively. These sensors were always calibrated before use with the standard calibration solutions (EC = 12.88 mS/cm; pH = 4.01, 7.0, and 9.0; redox = 240 mV; turbidity = 0, 20, and 100 FTU).

Water samples were collected for the major cations; namely, Na, K, Ca, Mg, as well as Fe, Mn, and As in 15 mL plastic vials (SARSTEDT®), after measuring the onsite parameters using a standard sampling protocol (Bhattacharya et al., 2002; Hasan et al., 2007; Rahman et al., 2014; van Breukelen et al., 2003; von Brömssen et al., 2008). The water was filtered using a 0.45 μm filter and preserved in the 15 mL plastic vial using 1% concentrated HNO_3 (69%ACS, Merck®). Likewise, water samples were collected for major anions, specifically Cl, Br, F, SO_4, NO_3, and NO_2, and stored in a 15 mL plastic vial after filtration. Cations alongside Fe, Mn, and As were analyzed with inductively coupled plasma (ICP) mass spectrometry (Analytik Jena model PlasmaQuant MS) after diluting the samples with acidified ultrapure water (1% v/v) to decrease conductivity to below 100 μS/cm. A standard reference material tagged SRM 1640a (National Institute of Standard & Technology) was run at the start and end of each batch analysis exerting blank samples. An internal standard mix of Li 6; Sc, Y, Ln, Tb (20 ppb) was added to correct any fluctuations during the ICP-MS analyses. Anions were analyzed with a *Metrohm*® 818 ion chromatograph equipped with a Metrosep A supp 5–150/4.0 column. Accuracy and precision were tested by measuring both standard and blank samples following a run of every ten samples. In addition, three filtered water samples were collected for dissolved organic carbon (DOC) in 30 mL plastic vials (*SARSTEDT*®) and preserved with a 1% concentrated HCl (van Breukelen et al., 2003). These samples were analyzed using a *Shimadzu*® TOC analyzer (NPOC: non-purgeable organic carbon) after the removal of dissolved CO_2 by placing the samples in a vortex for 60 s (van Breukelen et al., 2003). All chemical water analyses were performed at the water lab of Delft University of Technology, the Netherlands.

2.3. Sediment collection and geochemical analyses

Ten sediment samples were collected from the aquifer at site GMF11 every 1.5 m between 12.2 and 30.8 m below surface level (Fig. 2 and Table S1 in Supplement), whereas at site JJS91, samples were collected every 1.5 m between 6.5 and 27.0 m below surface level (Fig. S3 and Table S2 in Supplement). The modified split spoon method (von Brömssen et al., 2008) was used to collect these samples, whereby a length of 0.45 m and a diameter of 2.54 cm PVC pipes were used as a liner in the split spoon at the end of the drilling pipe. The hand-flapper and hammer technique were combined to perform the core drilling (Fig. S5 in Supplement). In this method, a 5 cm diameter hole was drilled by repeatedly lowering and raising the drilling pipes (Horneman et al., 2004). For collecting sediment cores at 1.5 m intervals, a split spoon was attached to the end of the pipe instead of a drilling cutter (von Brömssen et al., 2008). These core samples were sealed with wax at both ends immediately after collection from the drill holes to maintain anoxic conditions (Fig. S5 in Supplement). In addition to wax, these samples were secured with caps and plastic tapes at both ends (Fig. S5 in Supplement). After sealing, the samples were transferred to the laboratory of the Geology Department, University of Dhaka, and refrigerated at 4 °C. In the laboratory, the sediment cores were trimmed at both ends (~5 cm) to avoid the influence of the wax and potential oxidation effects. Afterwards, these cores were split into halves using a core cutter to retrieve sediments from the PVC pipes (Fig. S5 in Supplement). From the middle of the cores, approximately 450 g of sediment was taken and transferred into a glass beaker. These samples were weighed and placed in an oven to dry at 105 °C for 24 h. After drying, sediment samples were weighed again and preserved in airtight bottles for geochemical analyses.

The core samples were transferred for analyzing grain size distribution and total carbonates (TGA) to the Sediment Research laboratory at VU University Amsterdam, the Netherlands. In addition, the samples were transferred for determining the organic matter content, bulk, and trace elemental composition (e.g., S, Fe_2O_3, Al_2O_3, As) to the Bureau Veritas laboratories in Vancouver, Canada. Grain size distribution and clay fraction were analyzed to obtain information about the physical characteristics of the aquifer using Sympatec HELOS KR laser-diffraction (ranging from 0.15 to 2000 μm). The content of organic matter and calcium carbonate ($CaCO_3$) were measured using *LECO* thermogravimetric analysis (TGA; at 550 and 615–1000 °C). Bulk elemental concentrations were measured in XRF, and trace metals were measured in the ICP-MS by digestion utilizing Lithium Borate Fusion. The *LECOC/S* was used to determine the content of inorganic carbon and sulfur.

2.4. Calculation of geochemical parameters and mixing fractions

The content of pyrite (FeS_2), pyrite bounded Fe, reactive Fe, and non-pyrite reactive Fe were estimated from the bulk elemental composition of S, Fe_2O_3, and Al_2O_3 according to following equations (Griffioen et al., 2012; Kruisdijk and van Breukelen, 2021; Zuurbier et al., 2016):

$$FeS_2 = \left(0.5M_{FeS_2}/M_sS\right) \tag{1}$$

$$Fe_{py} = \left(0.5M_{Fe}/M_sS\right) \tag{2}$$

$$Fe_{TR} = \frac{2M_{Fe}}{M_{Fe_2O_3}}\left(Fe_2O_3 - 0.225Al_2O_3\right) \tag{3}$$

where M_{FeS_2}, M_{Fe} and M_s are the molecular weight of pyrite (g/mol), iron (g/mol), and sulfur (g/mol); and S is content of sulfur in % d.w.

The following equation determined the content of Fe-oxides which related to the calculated non-pyrite reactive Fe:

$$Fe_{reac} = \left(Fe_{TR} - Fe_{py}\right) \tag{4}$$

where the pyrite bounded Fe (Fe_{py}) and total reactive Fe (Fe_{TR}) were calculated using equations (2) and (3).

The cation exchange capacity (CEC) was estimated based on the clay fractions and organic matter percentage (Appelo and Postma, 2005). The formula used to calculate CEC is as follows:

$$CEC\left(\frac{meq}{kg}\right) = 7 \times (\%clay) + 35 \times (\%C) \tag{5}$$

where the fraction of clay (% d.w.) and content of organic carbon (% d.w.) are denoted as %clay and %C, respectively.

Conservative concentrations (i.e., not influenced by processes besides mixing) of various solutes in abstracted water were calculated using equation (7) based on mixing fractions of infiltration water and native groundwater (calculated using Cl concentrations, shown in equation (6)), and the endmember concentrations of infiltration water and native groundwater (Appelo and Postma, 2005). For every moment, the actual end-member concentrations were used in the calculations. Differences between calculated conservative concentrations and the actual observed concentrations indicate either consumption (e.g., precipitation, sorption, degradation) or production (e.g., dissolution, desorption) of specific constituents and aid in the interpretation of the hydrochemical data.

$$f_{Cl} = \frac{m_{Cl,abstracted} - m_{Cl,infiltration}}{m_{Cl,NGW} - m_{Cl,infiltration}} \tag{6}$$

where the Cl-based fraction of infiltration water in abstracted water is denoted as f_{Cl}, *measured concentrations of Cl in infiltration, native*

groundwater, and abstracted water are denoted as $m_{Cl,infiltration}$, $m_{Cl,NGW}$, *and* $m_{Cl,abstracted}$, *respectively.*

$$m_{i,mix} = f_{Cl} \times m_{i,NGW} + (1 - f_{Cl}) \times m_{i,infiltration} \quad (7)$$

where *the conservative mixing between infiltration and native groundwater is denoted by* m_{mix}, the Cl-based fraction of infiltration water in abstracted water is denoted as f_{Cl}, *the concentrations of a particular ion (i) for native groundwater and infiltration water are denoted as* $m_{i,NGW}$, *and* $m_{i,infiltration}$.

2.5. Data validation and outliers

During data processing, part of the onsite measurements (~<2%) and lab analyzed data (~<10%) showed results that were visually out of range compared to the general trends observed during the monitoring period (indicated with unfilled markers in Fig. S6). These data were considered outliers (~10%) due to non-identified artifacts and were removed, as shown in Figs. 3 and 4. These outliers might indicate either contamination during field sampling or interferences during laboratory analyses.

2.6. Geochemical modelling

For hydrochemical data processing, recorded onsite parameters and laboratory analyzed data were stored in excel files. Stored data were processed using python pandas scripts for visualization and data interpretation.

2.6.1. Inverse geochemical and mass balance modelling

Inverse geochemical modelling was performed using the USGS programme PHREEQC interactive 3.0 for Windows (Parkhurst and Appelo, 1999) to identify the governing hydrogeochemical processes at each MAR site (Fig. 1). An inverse geochemical model aims to determine which set(s) of hydrogeochemical reactions and to what extent (in terms of moles of reaction) can explain observed changes in water composition in a system, including optional mixing of different water types. Inverse geochemical models have been applied to determine, for example, processes, explaining water quality changes in landfill leachate plumes (Amirbahman et al., 1998; van Breukelen et al., 2003), and has been applied as well as to an ASR system (Antoniou et al., 2012). In this study, specifically, the inverse model was used to calculate the degree of mixing between infiltration water with native groundwater and subsequently to explain which reactions could identify the further changes in water composition, as observed in abstracted water (see Fig. 2).

In our inverse model, we chose to represent the abovementioned water types based on their median concentration levels. We considered the following reaction equations in the inverse models: oxidation of organic matter; oxidation of Fe (II); reduction of DO; reduction of SO_4; dissolution of the carbonate minerals: calcite, and siderite; precipitation of FeS; and cation-exchange of Ca and Na. Inverse models usually have difficulties finding a solution to the problem when concentrations of some constituents are not allowed to be adjusted to some degree in the model. The inverse models in this study could be obtained while allowing individual concentrations to be adjusted within max. 8% (for Cl, SO_4, and Na).

A simple mass balance was calculated for Mn and As to determine their (im)mobilization during storage because of the limitation of the inverse model. In this simple approach, the fractions of infiltrated and native groundwater in the abstracted water were calculated based on the concentrations of conservatively behaving Cl (Appelo and Postma, 2005). From there, the concentrations of all other solutes were calculated based on the assumption of conservative mixing, i.e., without reactions (equations (6) and (7)). The differences between the measured concentrations and these calculated conservative mixing concentrations were considered because of reactive processes in the aquifer.

2.6.2. Forward geochemical modelling

So-called forward batch models were developed using the same PHREEQC software to study the impact of individual hydrogeochemical processes on the chemical composition of the abstracted water and, specifically, its pH as a process parameter. In this model, the infiltration water and the native groundwater were first mixed in the proportions as calculated by the inverse model without the occurrence of any chemical reaction. Subsequently, one or more of the individual processes, in the amounts as calculated by the inverse model, were added to this mixture to assess the influence of those individual processes on the abstracted water quality.

3. Results and discussion

3.1. Geochemical characterization of aquifer sediments

Table 1 and Tables S1–2 in the supplement present the geochemical properties of the aquifer sediments at sites GMF11 and JJS91. The aquifer at site GMF11 is composed of unconsolidated and grey-colored fine sands and silts with a clay fraction of 2–3% (Table S1 in the supplement). These sediments were deposited during the Holocene (Goodbred and Kuehl, 2000). The contents of organic matter (0.25 ± 0.1% d.w.), total carbon (0.6 ± 0.1% d.w.), and sulfur (0.02 ± 0.0% d.w.) were similar to and within the range of previously reported values for Holocene sediments in the Bengal delta basin (Anawar et al., 2010; McArthur et al., 2004; Nickson et al., 2000; Seddique et al., 2008). The carbonate content (mean of 6.0 ± 1.2% d.w.) was relatively high for this region (Naus et al., 2019b). The As content ranged from 2.5 to 4.5 ppm. The average content (3.8 ± 0.8 ppm) was slightly lower than the average As content (4.7 ± 3.2 ppm) of the Bengal delta sediments (Anawar et al., 2003; Chakraborty et al., 2015). The average pyrite content (0.04 ± 0.1% d.w.) was relatively low compared to previously reported values (0.28 ± 0.06% d.w.) for the Bengal delta basins (Nickson et al., 2000). Average contents of Fe and Al oxides (Table 1) were observed within the range of previously reported values for this region (Bibi et al., 2006; Seddique et al., 2008). The calculated CEC ranged from 20.9 to 27.4 meq/kg throughout this sandy aquifer, and these values agree with the CEC values of finer sands (Lupker et al., 2016). The contents of geochemical properties at JJS91 were similar to those at GMF11, considering the variations in depth (Table 1). Average As content was relatively lower, and average pyrite content was comparatively higher at JJS91, while contents of Fe-oxides (1 ± 0.23 versus 0.9 ± 0.07) were similar (Table 1).

3.2. Year-round monitoring at site GMF11

Fig. 3 shows the weekly and monthly measured onsite parameters, particularly, daily infiltration/abstraction flow rate (a-a'), temperature (b-b'), turbidity (c-c'), EC (d-d'), pH (e-e'), DO (f-f'), and Alkalinity (j-j') for the various sampling points at GMF11, which are plotted against the entire monitoring period (December 5, 2017 to December 7, 2018). Furthermore, the concentrations of Cl (g-g'), Na (h-h'), Ca (i-i'), SO_4 (k-k'), Fe (l-l'), Mn (m-m'), and As (n-n') are also shown in Fig. 3. The grey shading in Fig. 3 indicates the monsoon period (June–October). Note that EC, Cl, Na, Ca, Fe, Mn, and As in pond and infiltration water are plotted on the secondary y-axes in Figs. 3 and 4. This was done to present better their lower concentration levels and variations over time.

3.2.1. Pond (source) water quality

At site GMF11, fresh surface water from the pond is used as source water after sand filtration and injected into the brackish, anoxic aquifer. During the monsoon, abundant rainfall and runoff from the neighboring surface areas mostly replenish this pond. Fig. 3 (d-d') shows that the pond contained fresh water, as indicated by the low EC values throughout the year. The EC even decreased slightly, but steadily, from 0.39 to 0.31 mS/cm during the monsoon (June–October). During the

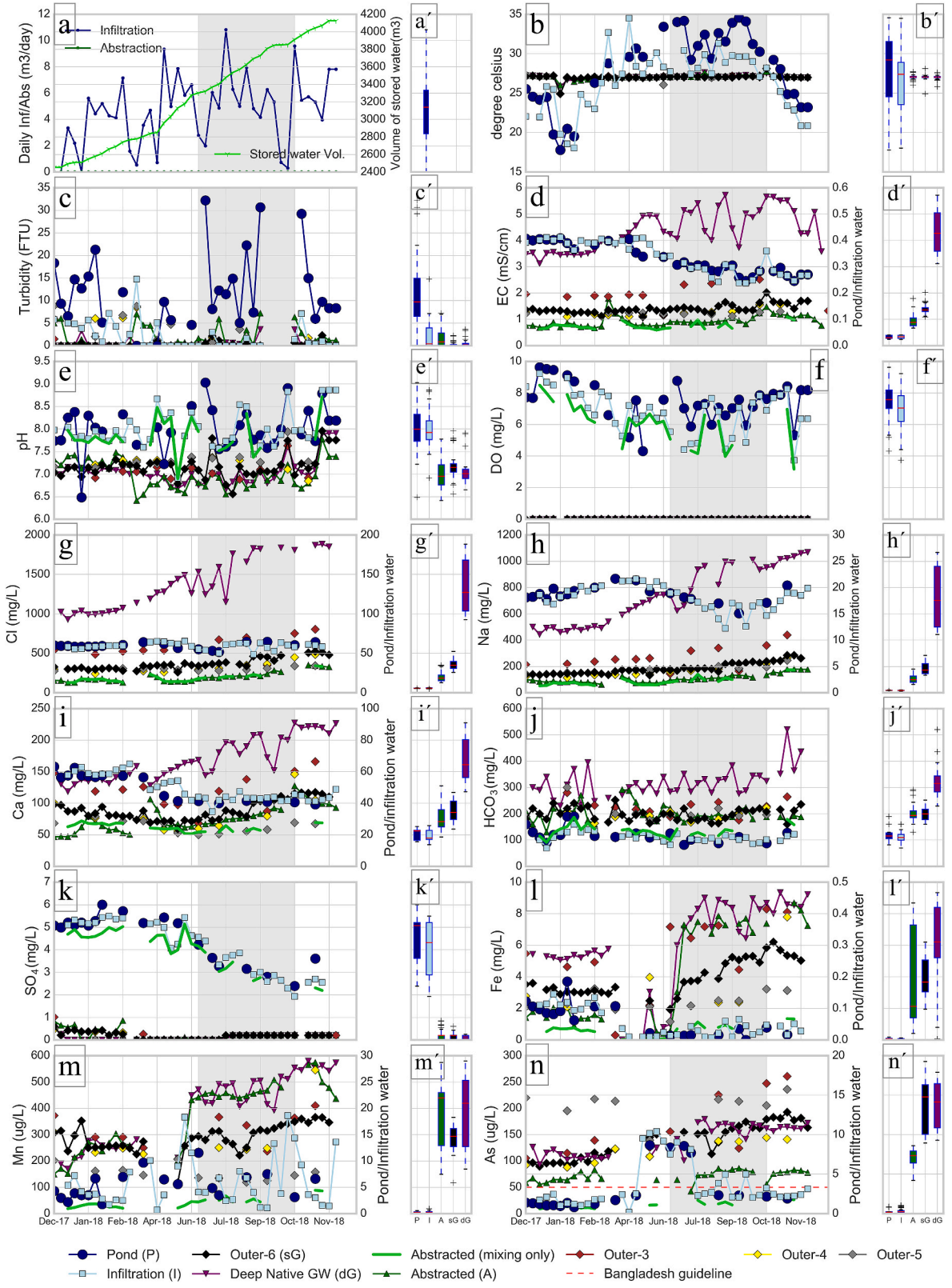

Fig. 3. (Columns 1 and 3) Measured onsite parameters daily infiltration/abstraction water volume (a), temperature (b), turbidity (c), electrical conductivity (EC, d), pH (e), DO (f) and concentrations of Cl (g), Na (h), Ca (i), Alkalinity (j), SO_4 (k), Fe (l), Mn (m), and As (n) during the monitoring period from 2017/12/05 to 2018/12/07 at site GMF11. (Columns 2 and 4) Box plots for the entire monitoring period illustrating the differences in levels for pond water, infiltration water, abstracted (recovered) water, and groundwater at the outer shallow and the deep monitoring wells (indicated by similar color used in column 1 and 3, and the same alphabet with the prime symbol used for each panel). Note that EC, Cl, Na, Ca, Fe, Mn, and As in pond and in infiltration water are plotted on the secondary y-axes. (For interpretation of the references to color in this figure legend, the reader is referred to the Web version of this article.)

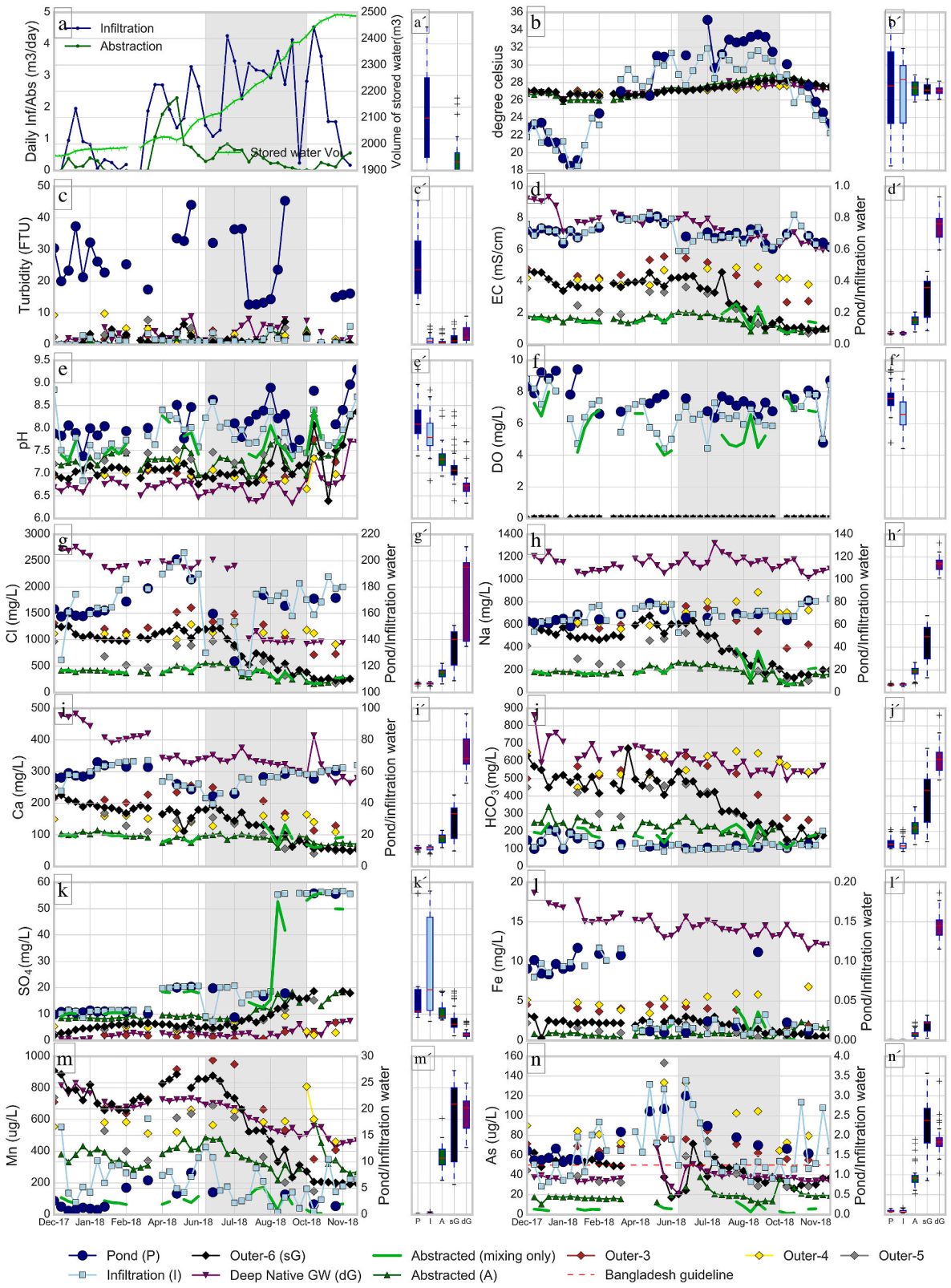

Fig. 4. (Columns 1 and 3) Measured onsite parameters daily infiltration/abstraction water volume (a), temperature (b), turbidity (c), electrical conductivity (EC, d), pH (e), DO (f), and the concentrations of Cl (g), Na (h), Ca (i), Alkalinity (j), SO_4 (k), Fe (l), Mn (m), and As (n) during the monitoring period from 2017/12/05 to 2018/12/06 at site JJS911. (Columns 2 and 4) Box plots for the entire monitoring period illustrating the differences in levels for pond water, infiltration water, abstracted (recovered) water, and groundwater at the outer shallow and the deep monitoring wells (indicated by similar color used in column 1 and 3, and the same alphabet with the prime symbol used for each panel). Note that EC, Cl, Na, Ca, Fe, Mn, and As in pond and in infiltration water are plotted on the secondary y-axes. (For interpretation of the references to color in this figure legend, the reader is referred to the Web version of this article.)

Table 1
Comparison between the geochemical characteristics (mean values) of the aquifer materials at site GMF11 and JJS911.

Parameters	Units	GMF11 (n = 4)	JJS91 (n = 4)
Clay fraction (<8 μm)	% d.w.	2.9 ± 0.5	3.0 ± 0.11
Very Fine Silt (8–16 μm)	% d.w.	16.2 ± 11.4	12.1 ± 7.5
Fine Silt (16–32 μm)	% d.w.	2.5 ± 1.5	3.2 ± 2.3
Silt (8–63 μm)	% d.w.	3.8 ± 2.0	5.3 ± 3.4
Very Fine Sand (63–125 μm)	% d.w.	78 ± 12.6	82.6 ± 10.8
Fine Sand (125–250 μm)	% d.w.	29.3 ± 6.7	23.2 ± 3.6
Sand (63–2000 μm)	% d.w.	9.6 ± 7.1	5.1 ± 2.5
SOM	% d.w.	0.25 ± 0.1	0.29 ± 0.12
$CaCO_3$	% d.w.	6.0 ± 1.2	4.7 ± 0.79
TOT/C	% d.w.	0.6 ± 0.1	0.5 ± 0.12
TOT/S	% d.w.	0.02 ± 0.0	0.04 ± 0.02
C/ORG	% d.w.	0.1 ± 0.04	0.15 ± 0.06
SiO_2	% d.w.	73 ± 2	74.5 ± 1.9
Al_2O_3	% d.w.	10 ± 0.7	10 ± 0.59
Fe_2O_3	% d.w.	3.8 ± 0.5	3.5 ± 0.21
As	ppm	3.8 ± 0.8	3.1 ± 0.56
CEC (calculated)	meq/kg	24 ± 2.8	26.2 ± 2.4
Pyrite (calculated)	% d.w.	0.04 ± 0.01	0.07 ± 0.03
Ferric Oxides (calculated)	% d.w.	1 ± 0.23	0.9 ± 0.07

monsoon, additional rainfall usually dilutes pre-existing pond water, which can explain the observed change in EC (Ayers et al., 2017). The major ions Na (19 ± 1.7 mg/L), Cl (59.6 ± 3.6 mg/L), Ca (50.3 ± 9 mg/L), SO_4 (4.6 ± 1.1 mg/L), and Mg (7.1 ± 0.6 mg/L) followed this seasonal variation of EC. The concentrations of NO_3 and PO_4 were steady and low (Table S3 in Supplement), which were similar to the reported concentrations of rainwater harvesting systems in the region (Ghosh et al., 2015). The mean concentrations of Fe (0.1 ± 0.05 mg/L), Mn (5.3 ± 2.5 μg/L), and As (3 ± 2.8 μg/L) remained nearly stable during the entire year (Table S3 in Supplement), except for the period of May–July 2018 ((Fig. 3l-n'). Some studies in SW Bangladesh have found similar and relatively higher As concentrations in freshwater ponds (Ayers et al., 2017; Islam et al., 2000, 2014). The pH was 8.0 ± 0.5 and remained steady throughout the period (Fig. 3e-e', Table S3 in Supplement). The pond water was turbid with a mean value of 12.4 ± 8.5 FTU and increased during the monsoon to 16 ± 10.1 FTU (Fig. 3c-c'). During the monsoon, direct rainfall in the pond is expected to lower turbidity. However, surface runoff carries suspended solids toward the pond, increasing turbidity, which has been observed in these areas (Islam et al., 2011, 2014). DOC was measured three times during the monitoring period, and the mean concentration (11.2 ± 1.4 mg/L) was within the measured range across the region (Ayers et al., 2017). The water was nearly saturated with DO throughout the monitoring period (7.5 ± 1.3 mg/L, ~91% of saturation concentration). However, it was somewhat lower during the monsoon (7.0 ± 0.9 mg/L; 92% of the saturation concentration). The comparatively higher turbidity and temperature in the monsoon (32.0 ± 1.9 °C) might have caused decreased DO levels in the surface water (Elbana et al., 2012).

3.2.2. Infiltration water quality

A sand filter was used to treat the pond water before injection, termed "infiltration water," in the following. EC values and concentrations of major ions remained almost identical for infiltration water throughout the year (Fig. 3d-d'). Therefore, it can be inferred that the pretreatment process has no impact on the major ion chemistry (Fig. 3g-k'), which is expected since conventional sand filters do not usually remove inert salts. However, the impact of the sand filter was noticeable for turbidity and DO (Fig. 3c-c', f-f'). The turbidity of pond water (mean value of 12.4 ± 8.5 FTU) decreased to 2.2 ± 3.2 FTU (~82% reduction) in the infiltration water (Table S3 in Supplement) as a consequence of suspended solids removal in the sand filter, in line with other conventional filters that remove suspended solids between 60 and 85% (Elbana et al., 2012). In addition, DO decreased from 7.5 ± 1.3 mg/L to 6.8 ± 1.4 mg/L, possibly due to the oxidation of biodegradable organic matter (Table S3 in Supplement). However, it is not feasible to make a direct comparison between pond and infiltration water as pond water samples were collected from the surface at the embankment, while the MAR system collects pond water (as a source of infiltration water) near the bottom of the pond (depth ~5 m) to ensure water availability throughout the year. As the pond's surface is exposed to atmospheric O_2 and sunlight during the daytime, algae growth is stimulated, enhancing DO levels. The lower DO levels in infiltration water could, therefore, also simply reflect the lower DO levels at the bottom compared to the surface of the pond. Low concentrations of NO_3 and PO_4 indicate low levels of human or animal pollution in both pond and infiltration water (Table S3 in Supplement).

3.2.3. Native (brackish) groundwater quality

The native groundwater pumped from the center deep well (depth of filter = 24.5–27.5 mbgl, Fig. 2) showed a steady increase in EC from 3.88 ± 0.6 to 4.77 ± 0.6 mS/cm during the monsoon (Fig. 3d-d'). The major ions Na (Fig. 3h-h'), Cl (Fig. 3g-g'), Ca (Fig. 3i-i'), HCO_3 (Fig. 3j-j'), Mg (Table S3 in Supplement), and K (Table S3 in Supplement) followed this change in EC. The increasing trend in EC over time suggests the occurrence of an upward flow of deeper saline groundwater, which may vary seasonally at this specific depth in the aquifer. The mean pH was 7.0 ± 0.3 and remained steady throughout the year (Fig. 3e-e'). The consistent concentrations of DO (Fig. 3f-f'), NO_3 (Table S3 in Supplement), and SO_4 (Fig. 3k-k') below the detection limit suggest that the native groundwater remained anaerobic with reducing conditions throughout the entire monitoring period. The temperature was stable with a mean value of 27.0 ± 0.3 °C (Fig. 3b-b'). The steady and low turbidity values (mean = 0.5 ± 1.0 FTU) indicate the water as clear upon abstraction (Sultana et al., 2015). DOC concentrations (13.6 ± 1.2 mg/L) were within the range but comparatively lower than the measured mean value (~25 mg/L) for the region (Ayers et al., 2017). The concentrations of Fe (6.0 ± 2.9 mg/L), Mn (0.40 ± 0.14 mg/L), and As (139 ± 28 μg/L) were relatively high (Islam et al., 2014). These elements showed higher concentration levels from the middle up to the end of the monitoring period than at the beginning (Fig. 3l–n'). The changes may relate to the earlier discussed possible inflow of deeper groundwater. The deeper groundwater may contain elevated levels of Fe, Mn, and As, explaining these increases over time.

3.2.4. Processes affecting abstracted (recovered) water quality

The infiltration of the filtered, aerobic freshwater that contained low concentrations of As and nutrients, e.g., NO_3 and PO_4, into the anaerobic brackish groundwater resulted in a freshwater bubble and triggered hydrogeochemical reactions, as discussed in the following. The freshwater bubble was abstracted afterwards using a hand-operated tube well (depth of screen = 18.0–21.5 mbgl, Fig. 2) for domestic purposes. The water was, however, restricted for drinking as the As concentration exceeded the Bangladesh drinking water standard of 50 μg/L, albeit As in infiltration water did not exceed a few μg/L. In the following, the governing processes are described and attempted to explain the water quality changes during storage and transfer.

(a) Mixing: The mean EC value of the abstracted water was 0.93 ± 0.23 mS/cm. The EC of the infiltration water (0.34 ± 0.06 mS/cm) thus increased by a factor of 2.7, but the EC of the abstracted water was still a factor 4.7 lower than the EC of native groundwater (Table S3 in Supplement). The systematic increase in EC of abstracted water compared to infiltration water suggests the occurrence of mixing with native brackish groundwater in the MAR system. Based on the EC values of infiltration water, abstracted water, and native groundwater, the proportion (i.e., the mixing fraction) of native groundwater and infiltration water composing the abstracted water was calculated and plotted in Fig. S7 in Supplementary material (Appelo and Postma, 2005).

Fig. S7 (in the supplement) shows that the fraction of native groundwater composing abstract water tends to increase from approximately 10%–20% over time. Because the salinity of the native groundwater increased by a factor of ~1.4 over the same period, and the salinity of abstraction water increased by a factor of ~1.3 at the end of the monitoring period compared to the beginning of the monitoring period. Thus, although steady infiltration (Fig. 3a-a') and absence of abstraction occurred in this MAR system, the salinity of the recovered water deteriorated. Based on the calculated conservative (mixing only) concentrations of abstracted water shown in Fig. 3 (green lines), SO_4 showed lower concentrations as would have been the result when only mixing occurred, whereas Alkalinity, Fe, Mn, and As displayed enhanced concentrations.

(b) Consumption of O_2 in aquifer: Fig. 3f-f' shows DO concentrations below the detection limit in the abstracted water, center deep well, and observation wells number 3–6, which indicates its consumption from the infiltration water (Table S3 in Supplement). Potential reductants causing DO consumption could be: pyrite, organic matter either as infiltrated from the pond (DOC) or as sedimentary organic matter (SOM) and dissolved as well as desorbed Fe^{2+} (Antoniou et al., 2012; Jin et al., 2016; Vanderzalm et al., 2011; Zuurbier et al., 2016).

Pyrite oxidation would result in increased SO_4 and Fe concentrations and can mobilize As in abstracted water (Antoniou et al., 2012; Zuurbier et al., 2016). Released Fe^{2+} can further react with DO and precipitates as $Fe(OH)_3$. These neo-formed Fe-oxides might create sorption sites for As and, as a result, immobilize the previously mobilized As (Wallis et al., 2011). However, comparatively low SO_4 concentrations (Fig. 3k-k') and low pyrite content were observed in aquifer sediments (Table 1) that rarely support the occurrence of pyrite oxidation and can be considered a minor process.

$$FeS_2 + \frac{7}{2}O_2 + H_2O \rightarrow Fe^{2+} + +2SO_4^{2-} + 2H^+ \quad (8)$$

$$4Fe^{2+} + O_2 + 10H_2O \rightarrow 4Fe(OH)_3 + 8H^+ \quad (9)$$

In addition to pyrite, the oxidation of organic matter may explain the DO consumption, which can be expected in shallow aquifers of the Bengal basin (Anawar et al., 2013; Hasan et al., 2007; McArthur et al., 2004). Organic matter is available as both DOC (9.5 ± 1.1 mg/L) in infiltration water and SOM (0.25 ± 0.1% d.w.) in the aquifer. The oxidation of organic matter would cause an increase in Alkalinity, which would agree with higher measured Alkalinity concentrations than its conservative mixing line (Fig. 3j-j'). However, the DOC concentration (9.5 ± 1.2 mg/L) in abstracted water was similar to DOC levels in infiltration water. Besides the SOM oxidation in the aquifer (which is the most likely to occur), the higher DOC levels in native groundwater and the mixing factor could still point to some DOC oxidation. It should be noted that (part of) the increased Alkalinity might also occur due to a drop in pH during the oxidation of organic matter and subsequent dissolution of the $CaCO_3$ (Appelo and Postma, 2005).

$$CH_2O + O_2 \rightarrow CO_2 + H_2O \quad (10a)$$

$$CO_2 + H_2O \rightarrow HCO_3^- + H^+ \quad (10b)$$

$$CO_2 + H_2O + CaCO_3 \rightarrow Ca^{2+} + 2HCO_3^- \quad (11)$$

The oxidation of dissolved Fe (in native groundwater) can also support the DO consumption at this site that subsequently precipitates as $Fe(OH)_3$ (Antoniou et al., 2012). This newly formed Fe $(OH)_3$ might adsorb dissolved As, Mn, and Fe, and as a result, concentrations of these elements are likely to be decreased. However, based on these monitoring data, the process of $Fe(OH)_3$ formation and change of the concentrations of Fe, Mn, and As in Fig. 3l–n' seem inconclusive.

(c) pH as process indicator: Fig. 3e-e' shows that pH (7.0 ± 0.3) fluctuates and is lower than its mixing line suggesting the occurrence of hydrogeochemical processes during storage. Several processes can change the pH either in a downward or upward direction. The pH may decrease due to the oxidation of DOC/SOM and Fe^{2+}, which precipitates as $Fe(OH)_3$. Furthermore, the produced CO_2 from DOC/SOM oxidation may react with $CaCO_3$, which upon dissolution, increases Alkalinity (equations (10) and (11)) and increases the pH (Appelo and Postma, 2005). Conversely, SO_4 reduction coupled to DOC/SOM oxidation would result in a subsequent pH drop (Appelo and Postma, 2005; McAllister et al., 2015; Sun et al., 2016). The changes in pH and associated processes likely influence the abstracted water quality, as will be further discussed in Section 3.4.

(d) Mobilization of Fe, Mn, and As: Fig. 3l–n' displays increased concentrations of Fe (4.3 ± 3.1 mg/L), Mn (370 ± 126 μg/L), and As (72 ± 11 μg/L) in the abstracted water, compared to their mixing lines that suggest the potential mobilization processes. The hydrogeochemical processes involved in DO consumption may have played a role in these mobilization processes. Moreover, the increased Alkalinity due to either SOM/NOM oxidation or $CaCO_3$ dissolution might induce the competitive desorption of As, Mn, and Fe from metal oxides surfaces (Appelo and de Vet, 2003; Rahman et al., 2014; Wallis et al., 2011). It should be noted that the Alkalinity in abstracted water is lower than in native groundwater, making competitive desorption by produced Alkalinity less likely. However, the decreased pH in the abstracted water suggests that $Fe(OH)_3$ precipitation was likely to occur and, to some extent, may have counteracted the mobilization of these elements.

3.3. Year-round monitoring data at JJS91

Pond and infiltration water: Compared to GMF11, a similar pond water quality was observed at JJS91 (Fig. 4a-n'), except for EC (comparatively higher: 0.70 ± 0.05 versus 0.33 ± 0.1 mS/cm), pH (slightly more alkaline: 8.2 ± 0.4 versus 8.0 ± 0.5), Fe (higher: 0.1 ± 0.04 versus 0.07 ± 0.05 mg/L), Mn (lower: 2.9 ± 2.2 versus 5.3 ± 2.5 μg/L), and As (lower: 1.8 ± 0.5 versus 2.9 ± 2.8 μg/L). Furthermore, SO_4 in the pond water was several times higher than at the other site (18 ± 14.3 versus 4.6 ± 1.1 mg/L), while it further increased during and after the monsoon (Fig. 4k-k' and Table S6 in supplement).

While the water quality of infiltration water was almost comparable to pond water (Fig. 4a-n'), the most distinct differences were observed for pH (decreased to 7.9 ± 0.4), DO (decreased to 6.7 ± 1.1 mg/L, ~12%), and turbidity (reduced to 4.2 ± 7.7 FTU, ~81%).

Native groundwater: The native groundwater at site JJS91 was similar to GMF11 in the sense that both were brackish and anaerobic. Comparatively, a higher EC (7.49 ± 0.92 versus 4.39 ± 0.77 mS/cm) was observed at this site, which, opposite to the other location, decreased over time, particularly after the monsoon. The major ions followed the EC trend of the native groundwater (Fig. 4a-n'). Compared to GMF11, a lower concentration of DOC (10.9 ± 0.1 versus 13.6 ± 1.2 mg/L) and a slightly acidic pH (6.7 ± 0.3 versus 7.0 ± 0.3) were observed at this site. In addition, comparatively higher concentrations were observed for Fe (14.5 ± 1.6 mg/L) and Mn (0.64 ± 0.11 mg/L), while relatively lower concentrations were observed for As (37.8 ± 7.1 μg/L) at this site. In addition, the concentrations of Fe, Mn, and As decreased (instead of increased) over time (Fig. 4i-n').

Abstracted water: Similar to GMF11, the stored freshwater was abstracted (depth of screen = 13.7–16.8 mbgl) and used for domestic as well as drinking water purposes at site JJS91. The mean value of EC was 1.5 ± 0.37 mS/cm, and the EC value of the infiltration water (0.71 ±

0.07 mS/cm) increased with a factor of 2.1 but was still a factor 5.1 lower than native groundwater (Table S5 in Supplement). The mixing fraction of native groundwater decreased from about 13% to about 5% during the monitoring period (Fig. S7 in Supplement). Therefore, this decreased mixing fraction and reduced levels of salinity and Fe, Mn, and As in native groundwater (Fig. 4i-n') positively affected the abstracted water quality (Fig. 4 and Fig. S7 in Supplement).

The changes of major ions and Fe, Mn, and As in relation to their mixing lines (Fig. 4a-n') were similar to those at the other site, except for Mg (Table S5 in Supplement) and Fe (Fig. 4l-l'). These elements showed decreased values compared to their mixing lines (Fig. 4l–l', Table S5 in Supplement). The other parameters were similar except for the pH. In contrast to GMF11, an increased pH (compared to native GW) was observed at this site (Fig. 4e-e'). The associated process/or processes for this pH change could not be comprehended directly from the monitoring data at this site and will be further discussed in section 3.5.

3.4. Geochemical modelling of site GMF11

Inverse and forward geochemical models of site GMF11 were made applying PHREEQC, based on the median concentration values of selected parameters of the infiltration water, the (deep) native groundwater, and the abstracted water, as shown in Table 2. The models simulated the abstracted water composition developed due to the mixing of infiltration water with native groundwater and additional hydrogeochemical processes.

Cl was used in the geochemical models as a key parameter to determine the degree of mixing between infiltration water and native groundwater. The Cl concentration in the abstracted water was between the infiltration and the native groundwater, agreeing with a mixing ratio of 89.5% infiltration water with 10.5% native groundwater. The saturation indices (SI) of calcite, dolomite, and siderite were calculated with PHREEQC after mixing infiltration water and native groundwater. Because of the presence of DO in the mixture, the redox potential was high, and therefore, in the model, it is assumed that Fe dominantly occurred as Fe(III). Thus, the calculated SI value for siderite was high in native groundwater. The calculated mineral saturation indices (SIs) show that both the infiltration and native groundwater were (super) saturated with respect to calcite ($CaCO_3$), while the native groundwater was also (super)saturated with respect to dolomite (Table 2). Mixing of these calcite-saturated waters with different partial pressures of carbon dioxide (pCO_2 values) (Table 2: 0.001 versus 0.03) is known to induce dissolution of $CaCO_3$, i.e., "mixing corrosion" (Appelo and Postma, 2005). The abstracted water was indeed sub-saturated with respect to $CaCO_3$ and dolomite, indicating that carbonate minerals may have dissolved during storage (Table 2). Siderite ($FeCO_3$) was supersaturated in both the native and the abstracted water, suggesting the potential occurrence of siderite in the aquifer. The following parameters showed lower concentrations in the abstracted water than expected based on conservative mixing: DO (dropped to zero), SO_4 (dropped to zero), K, and Mg; whereas Alkalinity, Ca, Na, Fe, Mn, and As showed higher concentrations (Table 2).

Table 3 shows the set of reactive processes with the calculated extent of reactions from the inverse model. The inverse model deduced that 1) DO consumption was coupled to dissolved Fe^{2+} oxidation with subsequent $Fe(OH)_3$ precipitation, while the model pointed to siderite as the source of Fe(II); 2) sulfate-reduction was coupled to both SOM and DOC

Table 3
Inverse geochemical model simulating the abstracted water composition at site GMF11, where the listed processes were added to a ~90%:10% mixture of infiltration water and native groundwater, respectively.

Reaction	Equation	Change (mmol/L)
Redox processes		
O_2 consumption	$O_2 + 4H^+ + 4e^- \rightarrow 2\,H_2O$	0.197
SO_4 reduction	$SO_4^{2-} + 9H^+ + 8e^- \rightarrow HS^- + 4H_2O$	0.036
Organic matter oxidation	$CH_2O + H_2O \rightarrow CO_2 + 4H^+ + 4e^-$	0.072
DOC oxidation (Table 2)	$CH_2O + H_2O \rightarrow CO_2 + 4H^+ + 4e^-$	0.030
SOM oxidation (calculated)	$CH_2O + H_2O \rightarrow CO_2 + 4H^+ + 4e^-$	0.042
Fe(II) oxidation	$Fe^{2+} \rightarrow Fe^{3+} + e^-$	
	$Fe^{3+} + 3H_2O \rightarrow Fe(OH)_3 + 3H^+$	0.788
Mineral reactions		
Siderite dissolution	$FeCO_3 \rightarrow Fe^{2+} + CO_3^{2-}$	0.861
Calcite dissolution	$CaCO_3 \rightarrow Ca^{2+} + CO_3^{2-}$	0.534
FeS precipitation	$Fe^{2+} + HS^- \rightarrow FeS + H^+$	0.036
Cation Exchange		
Na desorption	$NaX \rightarrow Na^+ + X^-$	0.283
Ca sorption	$Ca^{2+} + 2X^- \rightarrow CaX_2$	0.141

Table 2
Measured median concentrations with standard deviations of the infiltration water, the abstracted water, and the deep native groundwater at site GMF11. The saturation index (SI) is shown as well. All values are expressed as mmol/L except manganese and arsenic which are expressed as μmol/L.

Parameters	Infiltration water	Deep native GW	Conservative Mixing (Model)	Abstracted water	Reacted (Calculated)
pH	7.9 ± 0.4	7.0 ± 0.3	7.5	6.9 ± 0.3	−0.6
Alkalinity	1.8 ± 0.5	5.2 ± 0.9	2.2	3.2 ± 0.5	1.0
O_2	0.2 ± 0.04	0.0 ± 0.0	0.19	0.0 ± 0.0	−0.19
DOC[a]	0.79 ± 0.09	1.1 ± 0.1	0.83	0.79 ± 0.10	−0.04
Cl	1.7 ± 0.8	36.0 ± 9.3	5.3	5.3 ± 1.8	0.0
SO_4	0.04 ± 0.01	0.0 ± 0.0	0.04	0.0 ± 0.0	−0.04
Na	0.8 ± 0.1	31.4 ± 9.6	4.03	4.4 ± 1.5	0.37
K[a]	0.1 ± 0.02	0.24 ± 0.04	0.11	0.1 ± 0.01	−0.01
Ca	1.1 ± 0.2	4.1 ± 0.04	1.4	1.8 ± 0.5	0.40
Mg	0.3 ± 0.04	2.8 ± 0.6	0.55	0.5 ± 0.2	−0.05
Fe	0.0 ± 0.0	0.12 ± 0.05	0.01	0.05 ± 0.1	0.04
Mn[a]	0.07 ± 0.1	7.7 ± 2.5	0.88	8.0 ± 2.3	7.1
As[a]	0.03 ± 0.04	2.0 ± 0.4	0.24	0.99 ± 0.1	0.75
$SI_{Calcite}$	0.2	0.07	−0.10	−0.35	
$SI_{Dolomite}$	−0.04	0.12	−0.47	−1.12	
$SI_{Siderite}$[b]	na	0.86	0.26[c]	0.42	
pCO_2	0.001	0.03	0.00	0.02	

[a] Values were considered with the simple mass balance.
[b] Fe is considered to occur as Fe(II) in groundwater under anaerobic and pH neutral condition(Jensen et al., 1998; Lofts et al., 2008). SIs of siderite were calculated for groundwater where DO was below detection limit (<0.5 mg/L) and therefore Fe was assumed to occur as Fe(II).
[c] DO and pe in the input solutions of the geochemical models were set to zero and -4, respectively, with the goal that all Fe becomes Fe(II), and the SI of siderite can be calculated.

oxidation while producing H_2S that precipitated subsequently to FeS minerals; 3) freshening induced cation-exchange as reflected by Ca sorption and Na desorption, and 4) $CaCO_3$ dissolution induced by Ca sorption and the aforementioned mixing corrosion. The dissolution of $CaCO_3$ and siderite noticeably increased the Alkalinity of the abstraction water. Note that the inverse geochemical model calculated the total OM that oxidized. We assumed DOC oxidation as equal to calculated in Table 2, and the difference between OM and DOC oxidation as SOM oxidation.

Table 3 presents the set of hydrogeochemical processes that might have changed the composition and affected the pH of the abstracted water. We expected that the DO consumption and the reduction of Fe-hydroxides by DOC and/or SOM might cause enhanced Fe^{2+} levels during storage. However, those processes would have led to a much higher pH than the one observed. The model in Table 3 shows that the oxidation of dissolved Fe^{2+} and subsequent precipitation as $Fe(OH)_3$ resulted in a drop in pH (see reaction equations in Table 3). Furthermore, precipitation of FeS due to the sulfate-reduction can lead to a pH drop in the abstracted water (reaction equations in Table 3). Either the oxidation of DOC and/or SOM (Table 3) or the dissolution of carbonate minerals can result in increased Alkalinity in the abstracted water. Moreover, this process, in its turn, might increase the pH (Appelo and Postma, 2005). Desorption of Na (Table 4: 4.32 mM predicted, while 4.03 mM would result from mixing only) agreed with cation exchange processes, possibly triggered when freshwater was injected into brackish groundwater.

The inverse model simulated all parameters according to the observed pH change; however, Alkalinity was still too high (Table 4: 3.41 mM versus 3.18 mM). The simulated set of hydro-geochemical processes led to a lower pH (7.24; see Table 4) than the conservative mixing (7.46; Table 4) but still exceeded the observed pH (6.95). Therefore, a forward reaction model was made using PHREEQC to assess the impact of individual processes on the simulated water composition. When the forward model simulated less calcite dissolution (~20%) than the inverse model did, the pH (6.97; Table 4) was closer to the one observed, while the simulated Ca (1.59 mM) and Alkalinity (2.94 mM) were slightly lower than measured (Table 4).

The uncertainty in the spatial and temporal composition of the native groundwater influenced the obtained results. The fate of As and Mn were not simulated with these models. Instead, a mass balance calculation indicated that As and Mn concentrations in the abstracted water were higher than expected in the case of only mixing processes (Table 2). This suggests that As and Mn were mobilized during the freshwater storage.

Table 4
Forward simulation of the abstracted water composition based on the mixture of infiltration water and native groundwater at site GMF11. Model results are shown, where values are expressed as mmol/L.

Parameters	Observed	Model (Mixing only)	Model (Final inverse model)	Model (Less $CaCO_3$ dissolution)
Cl	5.34	5.31	5.31	5.31
pH	6.95	7.46	7.24	6.97
Alkalinity	3.18	2.18	3.41	2.94
O_2	0.00	0.19	0.01	0.00
Fe	0.05	0.01	0.05	0.05
SO_4	0.00	0.04	0.00	0.00
Na	4.40	4.03	4.32	4.32
Ca	1.82	1.43	1.83	1.59
Mg	0.52	0.55	0.55	0.55
$SI_{Calcite}$	−0.35	−0.09	−0.03	−0.41
$SI_{Dolomite}$	−1.12	−0.47	−0.46	−1.16
$SI_{Siderite}$	0.42	0.26[a]	0.84[a]	0.49
pCO_2	0.02	0.00	0.01	0.02

[a] DO and pe in the input solutions of the geochemical models were set to zero and -4, respectively, with the goal that all Fe becomes Fe(II), and the SI of siderite can be calculated.

The PHREEQC model did not imply the reduction of Fe-hydroxides, whereas sulfate-reduction and subsequent FeS precipitation might have lowered As levels by co-precipitation. In the abstracted water, the increased Alkalinity (compared to mixing) could have induced the competitive desorption of As and PO_4 from metal-oxides (Fig. 3 and Table S3 in Supplement). This could lead to net mobilization of As in the abstracted water (Appelo and de Vet, 2003; Rahman et al., 2014; Stollenwerk et al., 2007; Wallis et al., 2011). However, the Alkalinity is lower in abstracted water than in native groundwater, making this competitive desorption less probable. Table 2 indicates that Mn and As might have dissolved due to siderite dissolution besides Fe (Bhattacharya et al., 2009; Nath et al., 2011; Nickson et al., 2000; Reza et al., 2013). In shallow aquifers of Bangladesh, reductive dissolution of Fe hydro-oxides led to elevated levels of Fe, Mn, and As. In addition, oxidation of organic matter resulted in raised levels of HCO_3. Carbonate minerals, e.g., siderite, were precipitated due to the elevated levels of Fe, Mn, HCO_3, and adsorbed (dissolved) As on the surface of the siderite (Reza et al., 2013; Saha et al., 2020). However, As might have dissolved and mobilized during the dissolution of previously precipitated siderite at this site. The main reason for the As mobilization, though, seems simply to be the desorption of As sorbed to Fe-oxides in the aquifer after low-As infiltration water enters the aquifer (see section S2 and Table S9 in Supplementary material for details on the adjusted forward model).

3.5. Geochemical modelling at JJS91

The inverse and forward geochemical models of site JJS91 are presented in Tables 6 and 7, respectively, based on the median values of selected parameters listed in Table 5. The inverse model calculated from Cl concentrations in the water types that abstracted water is a mixture of about 90% infiltration water and 10% native brackish groundwater at this site, which is similar to site GMF11. In addition, the calculated saturation indices (SIs) showed that the infiltration, native, and abstracted water were saturated to slightly supersaturated with respect to calcite, dolomite, and siderite (except for infiltration water) (Table 5).

Table 6 provides the set of reactive processes and their extent of reaction from the inverse model of JJS91. With respect to GMF11, Fe(II) oxidation was not included in the model for JJS91. Furthermore, the direction (cation exchange) and the magnitude of the other processes differed (Tables 3 and 6): organic matter oxidation and sulfate reduction were observed at ~5 and ~2.5 times higher extent, respectively, whereas the sum of siderite and calcite dissolution was observed at ~3 times lower extent. The geochemical properties at both sites did not differ considerably and could not explain the varying sets of reactions as also observed in other studies (Kruisdijk and van Breukelen, 2021). However, the higher extent of sulfate reduction and organic matter oxidation was caused by the higher sulfate levels in the infiltration water used at site JJS91. The inverse model calculated a reaction of 0.37 mmol/L organic matter oxidation (Table 6), which could be attributed to 0.11 mmol/L DOC oxidation (as calculated from mixing in Table 5) and 0.26 mmol/L SOM oxidation as the difference between OM (calculated from the inverse model) and DOC oxidation (mixing calculation). SOM vs. DOC oxidation was dominant at site JJS91, whereas at site GMF11 SOM and DOC oxidation were both lower and of the same magnitude. Possibly after balancing the electron-transfers between electron-donors (DOC and SOM) and electron-acceptors (O_2 and SO_4), it can be inferred that half of the DOC was likely oxidized with DO and the remainder of DOC plus SOM with SO_4 (Table 6). In contrast to site GMF11, the cation exchange process at this site was observed in reverse between Na (sorption) and Ca (desorption) (Table 6). The observed rise in pH (as opposed to the decline at GMF11) in the abstracted water (compared to mixing only) seems related to the absence of Fe^{2+} oxidation and the higher oxidation of organic matter at this site (reaction equations in Table 6).

Table 7 shows the result of the forward model to assess the impact of individual processes (Table 6) on the pH change at site JJS91. The

Table 5
Measured median concentrations with standard deviations of the infiltration water, the abstracted water, and the deep native groundwater at site JJS91. The saturation index (SI) is shown as well. All values are expressed as mmol/L except manganese and arsenic which are expressed as μmol/L.

Parameters	Infiltration	Deep native GW	Conservative Mixing (Model)	Abstracted water	Reacted (Calculated)
pH	7.8	6.7	7.1	7.30	0.19
Alkalinity	1.9	10.0	2.7	3.6	0.9
O_2	0.2	0.0	0.18	0.00	−0.18
DOC[a]	0.8	0.9	0.8	0.72	−0.11
Cl	4.9	67.3	10.96	10.97	0.01
SO_4	0.2	0.02	0.18	0.09	−0.09
Na	3.0	49.8	7.5	7.9	0.4
K[a]	0.1	0.32	0.14	0.12	−0.02
Ca	1.5	8.6	2.2	2.3	0.19
Mg	0.75	5.4	1.2	1.2	−0.05
Fe[a]	0.0	0.26	0.03	0.01	−0.02
Mn[a]	0.1	12.3	1.3	6.5	5.2
As[a]	0.02	0.5	0.07	0.25	0.18
$SI_{Calcite}$	0.2	0.26	−0.24	0.10	
$SI_{Dolomite}$	0.28	0.48	−0.56	0.06	
$SI_{Siderite}$[b]	Na	1.03	0.24[c]	0.06	
pCO_2	0.002	0.10	0.01	0.01	

[a] Values were considered with the simple mass balance.
[b] Fe is considered to occur as Fe(II) in groundwater under anaerobic and pH neutral condition(Jensen et al., 1998; Lofts et al., 2008). SIs of siderite were calculated for groundwater where DO was below detection limit (<0.5 mg/L) and therefore Fe was assumed to occur as Fe(II).
[c] DO and pe in the input solutions of the geochemical models were set to zero and -4, respectively, with the goal that all Fe becomes Fe(II), and the SI of siderite can be calculated.

Table 6
Inverse geochemical model simulating the abstracted water composition at site JJS91, where the listed processes where added to a ~90%:10% mixture of infiltration water and native groundwater, respectively.

Reaction	Equation	Change (mmol/L)
Redox processes		
O_2 consumption	$O_2 + 4H^+ + 4e^- \rightarrow 2H_2O$	0.185
SO_4 reduction	$SO_4^{2-} + 9H^+ + 8e^- \rightarrow HS^- + 4H_2O$	0.093
Organic matter oxidation	$CH_2O + H_2O \rightarrow CO_2 + 4H^+ + 4e^-$	0.370
DOC oxidation (Table 5)	$CH_2O + H_2O \rightarrow CO_2 + 4H^+ + 4e^-$	0.110
SOM oxidation (calculated)	$CH_2O + H_2O \rightarrow CO_2 + 4H^+ + 4e^-$	0.260
Mineral reactions		
Siderite dissolution	$FeCO_3 \rightarrow Fe^{2+} + CO_3^{2-}$	0.077
Calcite dissolution	$CaCO_3 \rightarrow Ca^{2+} + CO_3^{2-}$	0.376
FeS precipitation	$Fe^{2+} + HS^- \rightarrow FeS + H^+$	0.093
Cation Exchange		
Na sorption	$Na^+ + X^- \rightarrow NaX$	0.403
Ca desorption	$CaX_2 \rightarrow Ca^{2+} + 2X^-$	0.201

Table 7
Forward simulation of the abstracted water composition based on the mixture of infiltration water and native groundwater at site JJS91. Model results are shown, where values are expressed as mmol/L.

Parameters	Observed	Model (Mixing only)	Model (Final inverse model)
Cl	10.97	10.96	10.96
pH	7.30	7.11	7.39
Alkalinity	3.61	2.68	3.61
O_2	0.00	0.18	0.00
Fe	0.01	0.03	0.01
SO_4	0.09	0.18	0.09
Na	7.94	7.53	7.94
Ca	2.34	2.15	2.32
Mg	1.15	1.20	1.20
$SI_{Calcite}$	0.10	−0.24	0.20
$SI_{Dolomite}$	0.06	−0.56	0.28
$SI_{Siderite}$	0.06	0.24[a]	0.07[a]
pCO_2	0.01	0.01	0.01

[a] DO and pe in the input solutions of the geochemical models were set to zero and -4, respectively, with the goal that all Fe becomes Fe(II), and the SI of siderite can be calculated.

simulated set of hydrogeochemical processes (Table 6) was more likely to cause a higher pH (7.39; see Table 7) than the conservative mixture (7.11; Table 7) and slightly exceeded the observed pH (7.30). The forward model very well simulated other parameters, including Alkalinity. Desorption of Ca (Table 7: 2.32 mM predicted, while 2.15 mM would result from mixing only) agrees with cation exchange processes that occur when freshwater is displaced by brackish groundwater at this site. Insufficient infiltration versus abstraction may have led to some salinization at this site. In contrast to GMF11, fresh water was infiltrated throughout the monitoring period, and abstraction was not executed because of high As levels that led to the freshening of the brackish aquifer, as reflected by the outcome of the inverse model of that site.

Similar to GMF11, the simple mass balance calculation in Table 5 suggests that As and Mn were mobilized during storage for the same reasons as elaborated at GMF11.

3.6. Discussion on the research approach and literature comparison of the key findings

A combined approach of weekly monitoring and geochemical modelling was applied to quantify the hydrogeochemical processes at the selected MAR sites. Collected water samples from all key locations (pond,infiltration water,native groundwater,abstracted water) in the MAR systems were analyzed weekly to observe the temporal and seasonal changes (monsoon). While interpreting this weekly monitored data, we closely observed the changes in water chemistry in each sampling location at each site. Although we could assume the occurrence of some hydrogeochemical processes with this interpretation, it was inconclusive to define the key hydrogeochemical processes during MAR with this approach. To this end, geochemical models were applied based on the median parameter values of the monitored period to determine and quantify the governing hydrogeochemical processes. The weekly monitored data brought insights into the systems' seasonal water quality variations. In contrast, the geochemical models allowed us to quantitatively determine the hydrogeochemical processes and make a stronger connection with the observed data.

The hydrogeochemical processes, such as oxygen consumption, oxidation of Fe and OM, reduction of SO_4, dissolution of carbonate minerals, and cation exchange that occurred at the studied locations were comparable to other ASR sites around the world (Antoniou et al., 2012; Fakhreddine et al., 2020, 2021; Naus et al., 2019b; Wallis et al., 2010, 2011; Zuurbier et al., 2016, 2017). In this study, DO from the fresh surface water was consumed during the infiltration and storage in the anaerobic aquifers. However, unlike ASR sites in the Netherlands (Antoniou et al., 2012, 2013; Zuurbier et al., 2014, 2016), where pyrite oxidation was most important, DO at the MAR sites in Bangladesh was (probably) primarily consumed by OM and, to a lesser extent, by dissolved Fe. During infiltration and storage, mixing of infiltration and native groundwater and geochemical reactions occurred that affect the water quality of abstracted water, as was previously observed (Fakhreddine et al., 2015, 2021). Freshening of brackish aquifers, and dissolution of minerals like calcite and siderite were observed similarly at other ASR sites across the world (Antoniou et al., 2012; Vanderzalm et al., 2010; Zuurbier et al., 2016).

The mobilization of As during MAR occurs as a result of the dissolution of As-bearing pyrite minerals due to the infiltration of aerobic water at many ASR sites around the world (Antoniou et al., 2012; Fakhreddine et al., 2015, 2021; Vanderzalm et al., 2011; Wallis et al., 2011; Zuurbier et al., 2016). During injection of DO into the underlying aquifers, introduced O_2 is consumed by the reductants like pyrite and can mobilize As and Fe. Under more oxidized conditions, dissolved Fe can further oxidize and limit the levels of As and Fe as they absorb on the newly precipitated $Fe(OH)_3$. However, at many MAR sites across South Asia (Fakhreddine et al., 2021; Mailloux et al., 2013; Polizzotto et al., 2005), As mobilizes under reducing conditions in the aquifer due to reductive dissolution of Fe-oxyhydroxides. During the storage and recovery phase, redox conditions shift towards more reduced conditions because of the depletion of DO. Subsequently, microbial-mediated reductive dissolution of Fe-oxyhydroxides can mobilize As and Fe in the recovered water. During infiltration and storage, the introduced DO was consumed by OM, which caused a pH drop, and in response, calcite dissolution occurred. Therefore, Alkalinity increased, and thus, higher concentrations of bicarbonate ions exchanged with Fe, Mn, and As on sorption sites of the iron oxides. However, this effect is probably limited as overall Alkalinity decreased in the aquifer because of freshwater infiltration. As might alternatively have dissolved and mobilized during siderite dissolution at both sites as explained before. Most likely, however, is that As is desorbed from the Fe-oxides in the aquifer in response to the inflow of low-As infiltration water, triggering re-equilibration with the surface sites and a net As desorption effect.

4. Implications of findings for abstracted water quality

The abstracted water quality depends on both hydrogeochemical processes and the mixing of infiltration water with native groundwater at both MAR sites. MAR design and operation should, in principle, enable abstraction of most of the infiltrated water without mixing with native groundwater. However, about 10% of the abstracted water originated from native groundwater, enhancing salinity and arsenic levels in abstracted water. The contributions of infiltration water, native groundwater, and hydrogeochemical processes to the levels of As and Mn in abstracted water were calculated based on the known mixing fractions and measured concentrations in Tables 2 and 5 (see also Tables S7–S8 in Supplement). With respect to As, roughly 20% originated due to mixing, while approximately 80% was caused by mobilization processes at both sites. With respect to Mn, these percentages contributed 20% and 80%, respectively at JJS91, and about 10% and 90%, at site GMF11. The occurrence of hydrogeochemical reactions, therefore, causes elevated As and Mn levels in the abstracted water. However, the raised levels of As and Mn can also be partially produced by mixing, whereas mixing itself had a minor but still relevant contribution. As a result, GMF11 did not comply with local drinking water standards.

The consumption of DO influenced water quality during storage. Limited infiltration (and abstraction) led to long residence times, allowing oxygen depletion that may negatively affect the precipitation of $Fe(OH)_3$. Re-equilibration of sorbed arsenic with the low arsenic infiltration water resulted in higher levels of As at both sites (compared to infiltration water), and water was not abstracted from GMF11 as the local guideline value was exceeded. Without abstraction, this situation can remain sustained for a long time as water is infiltrated around this pocket of stagnant poor-quality groundwater. A more enhanced and regular inflow of infiltration water and concurrent abstraction would 1) shorten the residence time of the stored water, possibly keeping conditions (sub)oxic; and 2) grow the size of the stored freshwater body limiting mixing with native groundwater in drinking water abstracted from its core. The regular inflow of DO from infiltration water can create new sorption sites for dissolved Fe, Mn, and As, which would lower their concentrations. Moreover, preventing mixing also excludes mixing corrosion and limits the dissolution of $CaCO_3$ and formation of Alkalinity, which possibly plays some role in As mobilization due to competitive desorption at these MAR sites. Despite similar contents of geochemical parameters such as SOM and carbonate content (Table 1), the hydrogeochemical responses were strikingly different at both sites because of the varied water chemistry of infiltration water and native groundwater, specifically with respect to the oxidation of dissolved Fe and organic matter (Tables 3 and 6). Aquifer geochemistry did not turn out as decisive in predicting abstracted water quality at these two locations.

5. Conclusion

The changes in water quality and the key hydrogeochemical processes were studied at two MAR sites in SW Bangladesh. During storage of infiltrated water, DO was consumed rapidly by dissolved Fe at GMF11 and by DOC/SOM at both sites. Moreover, DO consumption induced SO_4 reduction that was coupled to both DOC and SOM oxidation. The change of pH in the abstracted water at GMF11 (decreased) and at JJS91 (increased) suggests the occurrence of different hydrogeochemical reactions. At GMF11, precipitation of $Fe(OH)_3$ and FeS resulted in a pH drop, while siderite dissolution was considered as a source of dissolved Fe. At JJS91, the increase in pH occurred due to the increased Alkalinity and the absence of Fe(II) oxidation and subsequent precipitation of Fe $(OH)_3$. Alkalinity at this site increased because of DOC/SOM oxidation and $CaCO_3$ dissolution. Cation exchange between Ca (sorption) and Na (desorption) indicated that freshening of the brackish aquifer occurred due to steady freshwater infiltration at GMF11. In contrast, due to the inadequate infiltration compared to abstraction at JJS91, reversed cation exchange was observed between Ca (desorption) and Na (sorption). The mobilization of As occurred at both sites most likely due to desorption from Fe-oxides in response to the inflow of the low-As infiltration water. Furthermore, dissolution of As containing siderite may have played a role. Besides, the mixing of infiltration water with native groundwater resulted in increased salinity (EC) and levels of As and Mn in the abstracted water. When this mixing would be limited, the level of As and Mn in the abstracted water would lower and could further limit the dissolution of $CaCO_3$ (formation of Alkalinity) that may have contributed to As desorption. The regular inflow of fresh filtered pond water can enhance the size of the bubble and prevent the mixing with native groundwater, which can be achieved by maintaining a higher rate of infiltration and abstraction. This regular inflow of fresh aerobic water may curb the elevated levels of Fe, Mn, and As in the abstracted water due to the sorption on neo-formed Fe-oxides. Thus, the drinking water quality is expected to improve at these MAR systems in Bangladesh when these systems are differently designed and operated.

Declaration of competing interest

The authors declare that they have no known competing financial interests or personal relationships that could have appeared to influence the work reported in this paper.

Data availability

Data will be made available on request.

Acknowledgements

This work is part of the DeltaMAR project funded by the Urbanising Deltas of the World (UDW) programme of the Dutch Research Council NWO-WOTRO (Grant number: OND1357179). We gratefully acknowledge the support of Abir Delwaruzzaman in (weekly) sample collection and sediment core drilling. We want to thank Ayon Saha (University of Barishal) for his contribution (illustration) to the graphical abstract and schematic layout of MAR sites. Nadia van Pelt (Delft University of Technology) is also acknowledged for her notable contribution to English grammar revision. Finally, we thank the two anonymous reviewers for their comments which improved the quality of this manuscript.

Appendix A. Supplementary data

Supplementary data to this article can be found online at https://doi.org/10.1016/j.apgeochem.2022.105472.

References

Abedin, M.A., Collins, A.E., Habiba, U., Shaw, R., 2019. Climate Change, Water Scarcity, and Health Adaptation in Southwestern Coastal Bangladesh, vol. 10, pp. 28–42.
Alam, M., Sultana, M., Nair, G.B., Sack, R.B., Sack, D.A., Siddique, A.K., Ali, A., Huq, A., Colwell, R.R., 2006. Toxigenic Vibrio cholerae in the aquatic environment of Mathbaria, Bangladesh. Appl. Environ. Microbiol. 72, 2849.
Amirbahman, A., Schönenberger, R., Johnson, C.A., Sigg, L., 1998. Aqueous- and solid-phase biogeochemistry of a calcareous aquifer system downgradient from a Municipal solid waste landfill (winterthur, Switzerland). Environ. Sci. Technol. 32, 1933–1940.
Anawar, H.M., Akai, J., Komaki, K., Terao, H., Yoshioka, T., Ishizuka, T., Safiullah, S., Kato, K., 2003. Geochemical occurrence of arsenic in groundwater of Bangladesh: sources and mobilization processes. J. Geochem. Explor. 77, 109–131.
Anawar, H., Yoshioka, T., Konohira, E., Akai, J., Freitas, M., Tareq, S., 2010. Sources of organic carbon and depositional environment in the Bengal delta plain sediments during the Holocene period. Limnology 11, 133–142.
Anawar, H.M., Tareq, S.M., Ahmed, G., 2013. Is organic matter a source or redox driver or both for arsenic release in groundwater? Phys. Chem. Earth, Parts A/B/C 58–60, 49–56.
Annaduzzaman, M., Rietveld, L.C., Hoque, B.A., Bari, M.N., van Halem, D., 2020. Arsenic removal from iron-containing groundwater by delayed aeration in dual-media sand filters. J. Hazard Mater., 124823
Antoniou, E.A., van Breukelen, B.M., Putters, B., Stuyfzand, P.J., 2012. Hydrogeochemical patterns, processes and mass transfers during aquifer storage and recovery (ASR) in an anoxic sandy aquifer. Appl. Geochem. 27, 2435–2452.
Antoniou, E.A., Stuyfzand, P.J., van Breukelen, B.M., 2013. Reactive transport modeling of an aquifer storage and recovery (ASR) pilot to assess long-term water quality improvements and potential solutions. Appl. Geochem. 35, 173–186.
Appelo, C.A.J., de Vet, W.W.J.M., 2003. Modeling in situ iron removal from groundwater with trace elements such as as. In: Welch, A.H., Stollenwerk, K.G. (Eds.), Arsenic in Ground Water: Geochemistry and Occurrence. Springer US, Boston, MA, pp. 381–401.
Appelo, C.A.J., Postma, D., 2005. Geochemistry, Groundwater and Pollution, vol. 1996. A.A. BALKEMA PUBLISHERS.
Appelo, C.A.J., Drijver, B., Hekkenberg, R., de Jonge, M., 1999. Modeling in Situ Iron Removal from Ground Water, vol. 37, pp. 811–817.
Ayers, J.C., Goodbred, S., George, G., Fry, D., Benneyworth, L., Hornberger, G., Roy, K., Karim, M.R., Akter, F., 2016. Sources of salinity and arsenic in groundwater in southwest Bangladesh. Geochem. Trans. 17, 4.
Ayers, J.C., George, G., Fry, D., Benneyworth, L., Wilson, C., Auerbach, L., Roy, K., Karim, M.R., Akter, F., Goodbred, S., 2017. Salinization and arsenic contamination of surface water in southwest Bangladesh. Geochem. Trans. 18, 4.
Barker, J.L.B., Hassan, M.M., Sultana, S., Ahmed, K.M., Robinson, C.E., 2016. Numerical evaluation of community-scale aquifer storage, transfer and recovery technology: a case study from coastal Bangladesh. J. Hydrol. 540, 861–872.
Bhattacharya, P., Jacks, G., Ahmed, K.M., Routh, J., Khan, A.A., 2002. Arsenic in groundwater of the Bengal delta plain aquifers in Bangladesh. Bull. Environ. Contam. Toxicol. 69, 538–545.
Bhattacharya, P., Hasan, M.A., Sracek, O., Smith, E., Ahmed, K.M., von Brömssen, M., Huq, S.M.I., Naidu, R., 2009. Groundwater chemistry and arsenic mobilization in the Holocene flood plains in south-central Bangladesh. Environ. Geochem. Health 31, 23–43.
Bhuiyan, M.A.H., Rakib, M.A., Dampare, S.B., Ganyaglo, S., Suzuki, S., 2011. Surface water quality assessment in the central part of Bangladesh using multivariate analysis. KSCE J. Civ. Eng. 15, 995–1003.
Bibi, M.H., Ahmed, F., Ishiga, H., 2006. Distribution of arsenic and other trace elements in the Holocene sediments of the Meghna River Delta, Bangladesh. Environ. Geol. 50, 1243–1253.
Chakraborty, M., Mukherjee, A., Ahmed, K.M., 2015. A review of groundwater arsenic in the Bengal basin, Bangladesh and India: from source to sink. Curr. Pollut. Rep. 1, 220–247.
Dillon, P., Toze, S., Page, D., Vanderzalm, J., Bekele, E., Sidhu, J., Rinck-Pfeiffer, S., 2010. Managed aquifer recharge: rediscovering nature as a leading edge technology: water science and technology. J. Int. Assoc. Water Pollut. Res. 62, 2338–2345.
Dillon, P., Stuyfzand, P., Grischek, T., Lluria, M., Pyne, R.D.G., Jain, R.C., Bear, J., Schwarz, J., Wang, W., Fernandez, E., Stefan, C., Pettenati, M., van der Gun, J., Sprenger, C., Massmann, G., Scanlon, B.R., Xanke, J., Jokela, P., Zheng, Y., Rossetto, R., Shamrukh, M., Pavelic, P., Murray, E., Ross, A., Bonilla Valverde, J.P., Palma Nava, A., Ansems, N., Posavec, K., Ha, K., Martin, R., Sapiano, M., 2019. Sixty years of global progress in managed aquifer recharge. Hydrogeol. J. 27, 1–30.
Elbana, M., Ramírez de Cartagena, F., Puig-Bargués, J., 2012. Effectiveness of sand media filters for removing turbidity and recovering dissolved oxygen from a reclaimed effluent used for micro-irrigation. Agric. Water Manag. 111, 27–33.
Fakhreddine, S., Dittmar, J., Phipps, D., Dadakis, J., Fendorf, S., 2015. Geochemical triggers of arsenic mobilization during managed aquifer recharge. Environ. Sci. Technol. 49, 7802–7809.
Fakhreddine, S., Prommer, H., Gorelick, S.M., Dadakis, J., Fendorf, S., 2020. Controlling arsenic mobilization during managed aquifer recharge: the role of sediment heterogeneity. Environ. Sci. Technol. 54, 8728–8738.
Fakhreddine, S., Prommer, H., Scanlon, B.R., Ying, S.C., Nicot, J.-P., 2021. Mobilization of arsenic and other naturally occurring contaminants during managed aquifer recharge: a critical review. Environ. Sci. Technol. 55, 2208–2223.
Ghosh, G.C., Jahan, S., Chakraborty, B., Akter, A., 2015. Potential of household rainwater harvesting for drinking water supply. In: Hazard Prone Coastal area of Bangladesh, 14, pp. 937–942.
Goodbred, S.L., Kuehl, S.A., 2000. The significance of large sediment supply, active tectonism, and eustasy on margin sequence development: late Quaternary stratigraphy and evolution of the Ganges–Brahmaputra delta. Sediment. Geol. 133, 227–248.
Greskowiak, J., Prommer, H., Vanderzalm, J., Pavelic, P., Dillon, P., 2005. Modeling of Carbon Cycling and Biogeochemical Changes during Injection and Recovery of Reclaimed Water at Bolivar, vol. 41. Water Resources Research, South Australia.
Griffioen, J., Klein, J., van Gaans, P.F.M., 2012. Reaction capacity characterization of shallow sedimentary deposits in geologically different regions of The Netherlands. J. Contam. Hydrol. 127, 30–46.
Harvey, C.F., Swartz, C.H., Badruzzaman, A.B.M., Keon-Blute, N., Yu, W., Ali, M.A., Jay, J., Beckie, R., Niedan, V., Brabander, D., Oates, P.M., Ashfaque, K.N., Islam, S., Hemond, H.F., Ahmed, M.F., 2002. Arsenic mobility and groundwater extraction in Bangladesh. Science 298, 1602.
Hasan, M.A., Ahmed, K.M., Sracek, O., Bhattacharya, P., von Brömssen, M., Broms, S., Fogelström, J., Mazumder, M.L., Jacks, G., 2007. Arsenic in shallow groundwater of Bangladesh : investigations from three different physiographic settings. Hydrogeol. J. 15, 1507–1522.
Hasan, M.M., Ahmed, K.M., Sultana, S., Rahman, M.S., Ghosh, S.K., Ravenscroft, P., 2018. Investigations on groundwater buffering in khulna-satkhira coastal belt using managed aquifer recharge. In: Mukherjee, A. (Ed.), Groundwater of South Asia: Singapore. Springer Singapore, pp. 453–462.
Horneman, A., van Geen, A., Kent, D.V., Mathe, P.E., Zheng, Y., Dhar, R.K., O'Connell, S., Hoque, M.A., Aziz, Z., Shamsudduha, M., Seddique, A.A., Ahmed, K.M., 2004. Decoupling of as and Fe release to Bangladesh groundwater under reducing conditions. Part I: evidence from sediment profiles 1 1 Associate editor. G. Sposito: Geochem. Cosmochim. Acta 68, 3459–3473.
Ibrahim, K.M., El-Naqa, A.R., 2018. Inverse geochemical modeling of groundwater salinization in Azraq Basin, Jordan. Arabian J. Geosci. 11, 237.
Islam, M.R., Salminen, R., Lahermo, P.W., 2000. Arsenic and other toxic elemental contamination of groundwater, surface water and soil in Bangladesh and its possible effects on human health. Environ. Geochem. Health 22, 33–53.
Islam, M.A., Sakakibara, H., Karim, M.R., Sekine, M., Mahmud, Z.H., 2011. Bacteriological assessment of drinking water supply options in coastal areas of Bangladesh. J. Water Health 9, 415–428.
Islam, M.A., Karim, M.R., Higuchi, T., Sakakibara, H., Sekine, M.J.A.W.S., 2014. Comparison of the Trace Metal Concentration of Drinking Water Supply Options in Southwest Coastal Areas of Bangladesh, vol. 4, pp. 183–191.
Jensen, D.L., Boddum, J.K., Redemann, S., Christensen, T.H., 1998. Speciation of dissolved iron(II) and manganese(II) in a groundwater pollution plume. Environ. Sci. Technol. 32, 2657–2664.
Jin, J., Zimmerman, A.R., Norton, S.B., Annable, M.D., Harris, W.G., 2016. Arsenic release from Floridan Aquifer rock during incubations simulating aquifer storage and recovery operations. Sci. Total Environ. 551–552, 238–245.
Khan, A.E., Scheelbeek, P.F.D., Shilpi, A.B., Chan, Q., Mojumder, S.K., Rahman, A., Haines, A., Vineis, P., 2014. Salinity in drinking water and the risk of (Pre)Eclampsia and gestational hypertension in coastal Bangladesh: a case-control study. PLoS One 9, e108715.

Kruisdijk, E., van Breukelen, B.M., 2021. Reactive transport modelling of push-pull tests: a versatile approach to quantify aquifer reactivity. Appl. Geochem. 131, 104998.
Lofts, S., Tipping, E., Hamilton-Taylor, J., 2008. The chemical speciation of Fe(III) in freshwaters. Aquat. Geochem. 14, 337–358.
Lupker, M., France-Lanord, C., Lartiges, B., 2016. Impact of sediment-seawater cation exchange on Himalayan chemical weathering fluxes. Earth Surf. Dyn. Discuss. 1–15.
Mailloux, B.J., Trembath-Reichert, E., Cheung, J., Watson, M., Stute, M., Freyer, G.A., Ferguson, A.S., Ahmed, K.M., Alam, M.J., Buchholz, B.A., Thomas, J., Layton, A.C., Zheng, Y., Bostick, B.C., Geen, A.v., 2013. Advection of surface-derived organic carbon fuels microbial reduction in Bangladesh groundwater. Proc. Natl. Acad. Sci. USA 110, 5331–5335.
McAllister, S.M., Barnett, J.M., Heiss, J.W., Findlay, A.J., MacDonald, D.J., Dow, C.L., Luther III, G.W., Michael, H.A., Chan, C.S., 2015. Dynamic hydrologic and biogeochemical processes drive microbially enhanced iron and sulfur cycling within the intertidal mixing zone of a beach aquifer, 60, pp. 329–345.
McArthur, J.M., Banerjee, D.M., Hudson-Edwards, K.A., Mishra, R., Purohit, R., Ravenscroft, P., Cronin, A., Howarth, R.J., Chatterjee, A., Talukder, T., Lowry, D., Houghton, S., Chadha, D.K., 2004. Natural organic matter in sedimentary basins and its relation to arsenic in anoxic ground water: the example of West Bengal and its worldwide implications. Appl. Geochem. 19, 1255–1293.
Missimer, T., Maliva, R., 2010. Aquifer Storage and Recovery and Managed Aquifer Recharge Using Wells: Planning, Hydrogeology, Design, and Operation.
Morán-Ramírez, J., Ledesma-Ruiz, R., Mahlknecht, J., Ramos-Leal, J.A., 2016. Rock–water interactions and pollution processes in the volcanic aquifer system of Guadalajara, Mexico, using inverse geochemical modeling. Appl. Geochem. 68, 79–94.
Nath, B., Maity, J.P., Jean, J.-S., Birch, G., Kar, S., Yang, H.-J., Lee, M.-K., Hazra, R., Chatterjee, D., 2011. Geochemical characterization of arsenic-affected alluvial aquifers of the bengal delta (West Bengal and Bangladesh) and chianan plains (SW taiwan): implications for human health. Appl. Geochem. 26, 705–713.
Naus, F.L., Schot, P., Ahmed, K.M., Griffioen, J., 2019a. Influence of landscape features on the large variation of shallow groundwater salinity in southwestern Bangladesh. J. Hydrol. X 5, 100043.
Naus, F.L., Schot, P., Groen, K., Ahmed, K.M., Griffioen, J., 2019b. Groundwater salinity variation in Upazila Assasuni (southwestern Bangladesh), as steered by surface clay layer thickness, relative elevation and present-day land use: Hydrol. Earth Syst. Sci. 23, 1431–1451.
Naus, F.L., Schot, P., van Breukelen, B.M., Ahmed, K.M., Griffioen, J., 2021. Potential for managed aquifer recharge in southwestern Bangladesh based on social necessity and technical suitability. Hydrogeol. J. 29, 607–628.
Neil, C.W., Yang, Y.J., Jun, Y.-S., 2012. Arsenic mobilization and attenuation by mineral–water interactions: implications for managed aquifer recharge. J. Environ. Monit. 14, 1772–1788.
Nickson, R., McArthur, J., Burgess, W., Ahmed, K.M., Ravenscroft, P., Rahmanñ, M., 1998. Arsenic poisoning of Bangladesh groundwater. Nature 395, 338, 338.
Nickson, R.T., McArthur, J.M., Ravenscroft, P., Burgess, W.G., Ahmed, K.M., 2000. Mechanism of arsenic release to groundwater, Bangladesh and West Bengal. Appl. Geochem. 15, 403–413.
Page, D., Bekele, E., Vanderzalm, J., Sidhu, J., 2018. Managed Aquifer Recharge (MAR) in Sustainable Urban Water Management, 10, p. 239.
Poetra, R.P., Adji, T.N., Santosa, L.W., Khakhim, N., 2020. Hydrogeochemical conditions in groundwater systems with various geomorphological units in kulonprogo regency, Java Island, Indonesia. Aquat. Geochem. 26, 421–454.
Polizzotto, M.L., Harvey, C.F., Sutton, S.R., Fendorf, S., 2005. Processes conducive to the release and transport of arsenic into aquifers of Bangladesh. Proc. Natl. Acad. Sci. USA 102, 18819–18823.
Pyne, R.D.G., 2005. Aquifer Storage Recovery: a Guide to Groundwater Recharge through Wells. ASR systems.
Pyne, R.D., 2017. Groundwater Recharge and Wells: a Guide to Aquifer Storage Recovery. Routledge.
Rahman, M., Bakker, M., Borges Freitas, S., Halem, D., van Breukelen, B., Ahmed, K.M., Badruzzaman, A., 2014. Exploratory Experiments to Determine the Effect of Alternative Operations on the Efficiency of Subsurface Arsenic Removal in Rural Bangladesh, vol. 23.
Rahman, M.M., Bakker, M., Patty, C.H.L., Hassan, Z., Röling, W.F.M., Ahmed, K.M., van Breukelen, B.M., 2015. Reactive transport modeling of subsurface arsenic removal systems in rural Bangladesh. Sci. Total Environ. 537, 277–293.
Reza, A.H.M.S., Jean, J.-S., Bundschuh, J., Liu, C.-C., Yang, H.-J., Lee, C.-Y., 2013. Vertical geochemical variations and arsenic mobilization in the shallow alluvial aquifers of the Chapai-Nawabganj District, northwestern Bangladesh: implication of siderite precipitation. Environ. Earth Sci. 68, 1255–1270.
Saha, N., Bodrud-Doza, M., Islam, A.R.M.T., Begum, B.A., Rahman, M.S., 2020. Hydrogeochemical evolution of shallow and deeper aquifers in central Bangladesh: arsenic mobilization process and health risk implications from the potable use of groundwater. Environ. Earth Sci. 79, 477.
Seddique, A.A., Masuda, H., Mitamura, M., Shinoda, K., Yamanaka, T., Itai, T., Maruoka, T., Uesugi, K., Ahmed, K.M., Biswas, D.K., 2008. Arsenic release from biotite into a Holocene groundwater aquifer in Bangladesh. Appl. Geochem. 23, 2236–2248.
Stollenwerk, K.G., Breit, G.N., Welch, A.H., Yount, J.C., Whitney, J.W., Foster, A.L., Uddin, M.N., Majumder, R.K., Ahmed, N., 2007. Arsenic attenuation by oxidized aquifer sediments in Bangladesh. Sci. Total Environ. 379, 133–150.
Stuyfzand, P.J., 1998. Quality Changes upon Injection into Anoxic Aquifers in the Netherlands: Evaluation of 1 1 Experirnents: Attificial Recharge of Groundwate, pp. 283–291.
Sultana, S., Ahmed, K.M., Mahtab-Ul-Alam, S.M., Hasan, M., Tuinhof, A., Ghosh, S.K., Rahman, M.S., Ravenscroft, P., Zheng, Y., 2015. Low-Cost Aquifer Storage and Recovery: Implications for Improving Drinking Water Access for Rural Communities in Coastal Bangladesh, vol. 20, p. B5014007.
Sun, J., Quicksall, A.N., Chillrud, S.N., Mailloux, B.J., Bostick, B.C., 2016. Arsenic mobilization from sediments in microcosms under sulfate reduction. Chemosphere 153, 254–261.
van Breukelen, B., Röling, W., Groen, J., Griffioen, J., W van Verseveld, H., 2003. Biogeochemistry and Isotope Geochemistry of a Landfill Leachate Plume, vol. 65, pp. 245–268.
van Halem, D., Heijman, S.G.J., Johnston, R., Huq, I.M., Ghosh, S.K., Verberk, J.Q.J.C., Amy, G.L., van Dijk, J.C., 2010. Subsurface iron and arsenic removal: low-cost technology for community-based water supply in Bangladesh. Water Sci. Technol. 62, 2702–2709.
Vanderzalm, J.L., Page, D.W., Barry, K.E., Dillon, P.J., 2010. A comparison of the geochemical response to different managed aquifer recharge operations for injection of urban stormwater in a carbonate aquifer. Appl. Geochem. 25, 1350–1360.
Vanderzalm, J.L., Dillon, P.J., Barry, K.E., Miotlinski, K., Kirby, J.K., Le Gal La Salle, C., 2011. Arsenic mobility and impact on recovered water quality during aquifer storage and recovery using reclaimed water in a carbonate aquifer. Appl. Geochem. 26, 1946–1955.
von Brömssen, M., Häller Larsson, S., Bhattacharya, P., Hasan, M.A., Ahmed, K.M., Jakariya, M., Sikder, M.A., Sracek, O., Bivén, A., Doušová, B., Patriarca, C., Thunvik, R., Jacks, G., 2008. Geochemical characterisation of shallow aquifer sediments of Matlab Upazila, Southeastern Bangladesh — implications for targeting low-As aquifers. J. Contam. Hydrol. 99, 137–149.
Wallis, I., Prommer, H., Simmons, C.T., Post, V., Stuyfzand, P.J., 2010. Evaluation of conceptual and numerical models for arsenic mobilization and attenuation during managed aquifer recharge. Environ. Sci. Technol. 44, 5035–5041.
Wallis, I., Prommer, H., Pichler, T., Post, V., Norton, S.B., Annable, M.D., Simmons, C.T., 2011. Process-based reactive transport model to quantify arsenic mobility during aquifer storage and recovery of potable water. Environ. Sci. Technol. 45, 6924–6931.
Zuurbier, K.G., Zaadnoordijk, W.J., Stuyfzand, P.J., 2014. How multiple partially penetrating wells improve the freshwater recovery of coastal aquifer storage and recovery (ASR) systems: a field and modeling study. J. Hydrol. 509, 430–441.
Zuurbier, K.G., Hartog, N., Stuyfzand, P.J., 2016. Reactive transport impacts on recovered freshwater quality during multiple partially penetrating wells (MPPW-) ASR in a brackish heterogeneous aquifer. Appl. Geochem. 71, 35–47.
Zuurbier, K.G., Raat, K.J., Paalman, M., Oosterhof, A.T., Stuyfzand, P.J., 2017. How subsurface water technologies (SWT) can provide robust, effective, and cost-efficient solutions for freshwater Management in coastal Zones, 31, pp. 671–687.